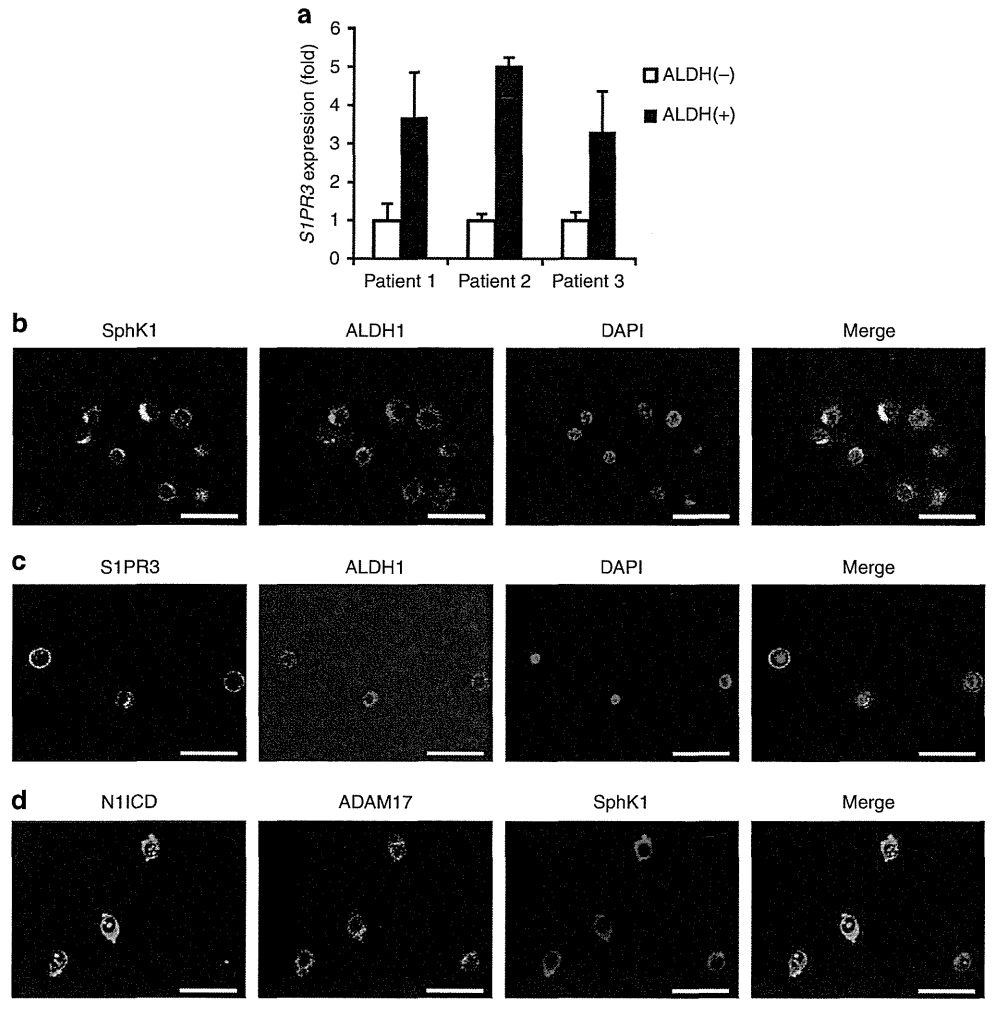

Figure 7 | SphK1-positive CSCs in human breast cancers. (**a**) *S1PR3* expression in the ALDH-negative or ALDH-positive patient-derived cells by qPCR. Expression levels were normalized to glyceraldehyde 3-phosphate dehydrogenase messenger RNAs. Data represent mean ± s.d. ($n=3$). (**b**) Double immunostaining of SphK1 (green) and ALDH1 (red) in patient-derived tumour cells. Nuclei were counterstained by DAPI (blue). (**c**) Double immunostaining of S1PR3 (green) and ALDH1 (red) in patient-derived tumour cells. Nuclei were counterstained by DAPI (blue). (**d**) Triple immunostaining of N1ICD (green), ADAM17 (red) and SphK1 (blue) in patient-derived tumour cells. Scale bar, 20 μm.

between the S1PR and ADAM17 activation in Notch ligands-independent manner. Further studies should be conducted looking at how the Notch system induces CSC phenotypes in breast cancer.

Our data demonstrate an essential cell autonomous role of Notch1 in breast CSCs expansion. Harrison *et al.*[42] has reported that Notch4 also affects breast CSCs. They performed knockdown of Notch paralog (Notch1 and Notch4) using both $ESA^+/CD44^+/CD24^{low}$ and mammosphere prepared from MCF-7 cells, although Notch ICD overexpression was not examined. Notch1 knockdown reduced only mammosphere population, whereas Notch4 knockdown reduced both $ESA^+/CD44^+/CD24^{low}$ and mammosphere populations (as shown in Figs 3a and 4b). Because Ginestier *et al.*[4] have already reported that two stem-like cell populations defined by ALDH positive and $CD44^+/CD24^-/lin^-$ were not identical, there is a possibility that discrepancy between our present data and Harrison's report is caused by the differences of cell populations used in the experiments. Thus, Notch paralog possibly plays a role in regulation in different stem cell population.

Our clinical samples suggest the crosstalk between Sphk1-S1P-S1PR3 and Notch signalling by co-localization of the components for the crosstalk machinery. Similar observations were obtained using xenografted tumour samples in nude mice. SphK1 has been already shown to be upregulated in patients with breast cancer[43], and its expression correlates with cancer progression and poor prognosis[43–45]. In addition, S1PR3 is the most highly expressed S1PR in breast cancer cells[46]. Thus, our data provide a potential explanation for significance of Sphk1-S1PR3-Notch axis in breast cancer.

Targeting Notch has been expected to facilitate tumour regression[47]. Although several types of Notch inhibitors are quite effective in preclinical models[21,48,49], none of the clinical trials conducted so far has examined effectiveness[50]. This prompts us to encourage efforts to explore alternative/additional approaches for targeting Notch. Our evidence suggests that Notch1 is involved in the S1P-induced CSC phenotype. Because lipid signalling acts upstream of the Notch, S1PR3 could be a promising target for various cancer. Indeed, TY52156 inhibited the tumorigenicity of SphK1-overexpressing breast CSCs (Fig. 6). Although several S1PR antagonists are currently available[14], few have been tested in clinical trials. The feasibility of S1PR3 antagonists in cancer remains to be determined.

In conclusion, the identification of S1P-derived CSC phenotype is required for continuous tumour growth, and points to potential

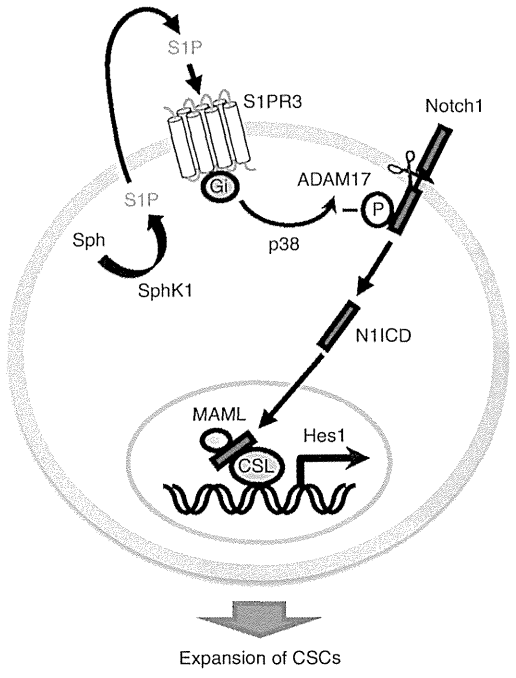

Figure 8 | A working model for the functions of SphK/S1P/S1PR3 in CSC regulation. S1P produced by SphK1 stimulates S1PR3 and subsequently activates Notch signaling in a Notch ligand-independent manner. Activation of S1P signaling pathway leads to expansion of CSCs.

culprits of tumour formation in patients. In the future, it might be possible to establish specific treatments that reduce tumorigenesis by targeting 'stemness' in cancer. Thus, efforts should be made to develop drugs capable of inhibiting CSC self-renewal and expansion by S1PR3.

Methods

Materials. Antibodies to p38MAPK (#9212), phospho-p38MAPK (#9211), Akt (#9272), phospho-Akt (#9271), Notch1 (#4380), N1ICD (#2421) and Notch3 (#2889) were from Cell Signaling Technology. Antibodies to HA (#H6908), FLAG (M2) (#F1804), myc (#C3956), β-actin (#A5441) and ADAM17 (phospho-Thr735) (#SAB4504073) were from Sigma-Aldrich. Antibody to ADAM17 (#AB19027) was from Millipore. Antibody to APC-conjugated TRA-1-85 (#FAB3195A) was from R&D Systems. Antibody to SphK1 (#AP7237c) was from Abgent. Antibody to ALDH1 (#611194), FITC mouse anti-human CD44 (#555478), PE mouse anti-human CD24 (#555428), FITC mouse IgG2b κ isotype control (#555742) and PE mouse IgG2a κ isotype control (#555574) were from BD Biosciences. Antibodies to S1PR2 (#sc-25491), S1PR3 (#sc-30024) and Spns2 (#130102) were from Santa Cruz Biotechnology. Antibody to SphK1 (#ab46719), ADAM17 (#ab57484), activated Notch1 (#ab8925) and ABCC1 (#ab3368) were from Abcam. Antibody to Alexa488-conjugated anti-rabbit IgG (#A11034) and Alexa555-conjugated anti-mouse IgG (#A21424) were from Invitrogen. S1P, dihydro-S1P, DAPT, SB203580, 5-Fluorouracil and doxorubicin were from Enzo Life Sciences. CAY10444, JTE013, MK571, LY294002, cyclopamine were from Cayman Chemicals. LPA was from Avanti Polar Lipids. Jagged1-Fc, Sonic hedgehog and Wnt3a were from R&D Systems. Botulinum C3 enzyme was from Bio Academia. PTX were from Wako Pure Chemical (Osaka, Japan). Hoechst, reserpine, DFO and PNU74654 were from Sigma-Aldrich, while N,N′-bis(4-chlorophenyl)-3,3-dimethyl-2-oxobutanehydrazonamide (TY52156) was synthesized. All other reagents were of analytical grade and obtained from commercial sources.

Cell culture. MCF-7 cells (American Type Culture Collection), MDA-MB-231 cells (American Type Culture Collection), A549 cells (European Collection of Cell Cultures) and LNCaP cells (European Collection of Cell Cultures), U251 cells (Japanese Collection of Research Biosources) were cultured in Dulbecco's modified Eagle's medium (DMEM; Sigma-Aldrich) supplemented with 10% heat-inactivated fetal bovine serum (FBS; Biological Industries), 100 U ml^{-1} penicillin and 100 μg ml^{-1} streptomycin (Gibco BRL). OVCAR-5 cells was cultured in RPMI1640 (Sigma-Aldrich) supplemented with 10% heat-inactivated FBS (Biological Industries), 100 U ml^{-1} penicillin and 100 μg ml^{-1} streptomycin (Gibco BRL).

Plasmid constructs and reporter assays. Plasmids encoding SphK1, SphK2, DN-CSL, DN-MAML, N1ICD, ADAM10 and 12xCSL-luc were kindly provided from Drs Stuart M. Pitson (University of Adelaide), Taro Okada (Kobe University), Aly Karsan (British Columbia Cancer Research Centre), Anthony J. Capobianco (University of Pennsylvania), Spyros Artavanis-Tsakonas (Harvard Medical School), Stefan Lichtenthaler (Ludvig Maximilians University) and Lothar J. Strobl (German Research Center for Environmental Health), respectively. Plasmids encoding N2ICD, N3ICD and N4ICD were kindly provided by Dr Michael J. Hendzel (University of Alberta). Plasmids encoding ADAM17 and DN-ADAM17 were kindly provided by Dr Rik Derynck (University of California, San Francisco). Plasmids encoding CA-G_i and CA-G_{12} were kindly provided by Dr J. Silvio Gutkind (National Institutes of Health). Plasmids encoding the ADAM17 mutants T735A and T761A were generated by QuikChange Site-Directed Mutagenesis (Stratagene) using pRK5-ADAM17-myc. A plasmid encoding the ADAM10 mutant E384A (DN-ADAM10) was generated by QuikChange Site-Directed Mutagenesis using peak-12-ADAM10-HA. Coding DNA sequences were verified by DNA sequencing. Transfections were conducted with FuGENE HD transfection reagent (Promega). Luciferase activity was assayed 24 h after transfection with 12xCSL-luc using the Glo Luciferase Assay Kit (Promega).

Microarray analysis. Total RNAs were isolated by Trizol (Invitrogen) and then purified using an RNeasy Mini Kit (Qiagen). Affymetrix Genome U133A gene chips (Affymetrix) were used to examine gene expression patterns according to the manufacturer's instruction. Genes upregulated more than twofold are shown in Supplementary Data 1.

ALDH assays. The ALDEFLUOR kit (Stem Cell Technologies) was used to detect CSC populations with high ALDH enzyme activity according to the manufacture's instruction[18]. The cells were plated at a density of 3×10^5 cells in 100 mm culture dishes. After serum deprivation for 3 days, cells were suspended at a concentration of 1×10^6 cells ml^{-1} in ALDH assay buffer containing the ALDH substrate BAAA (1 μM) and incubated for 30 min at 37 °C. As a negative control, cells were treated with diethylaminobenzaldehyde (15 μM), a specific ALDH inhibitor. A FACS Aria II cell sorter (BD Biosciences) was used to measure the ALDH-positive cell population.

Mammosphere-forming assays. MCF-7 cells were plated as single cells on ultralow attachment 6-well plates (Corning) at a concentration of 10,000 cells ml^{-1} in serum-free DMEM supplemented with N_2 supplement (Gibco) and 20 ng ml^{-1} basic Fibroblast Growth Factor (R&D Systems). After 4 days, the number of mammospheres was microscopically counted and the percentage of mammosphere-forming cells was determined as mammosphere-forming efficiency (%)[7].

SP assays. Cells were collected and suspended in prewarmed DMEM containing 2% FBS and 2 mM HEPES buffer. Hoechst 33342 dye (Sigma-Aldrich) was then added to a final concentration of 5 μg ml^{-1}, and the mixture was incubated with intermittent shaking for 60 min at 37 °C in the presence or absence of reserpine (15 μg ml^{-1}; Sigma-Aldrich). Cells were then resuspended in ice-cold phosphate-buffered saline (PBS) containing 2% FBS, and analysed with a FACS Aria II cell sorter (BD Biosciences).

CD44$^+$/CD24$^-$ cell population. Cells were resuspended in PBS containing 5% FBS and incubated with FITC mouse anti-human CD44 (#555478, 1:5) and PE mouse anti-human CD24 (#555428, 1:5) for 15 min at 4 °C. FITC mouse IgG2b κ isotype control (#555742, 1:5) and PE mouse IgG2a κ isotype control (#555574, 1:5) were used as negative control. Analysis was performed using a FACS Aria II cell sorter (BD Biosciences).

Cell viability assays. MCF-7 cells and sorted ALDH-positive cells were plated onto 96-well plates at a density of 5,000 cells well^{-1}. After overnight culture, cells were treated with 100 μM 5-Fluorouracil or 10 μM doxorubicin. After 72 h, MTS assays were performed, according to the manufacturer's instruction (Promega).

qPCR assays. Total RNA was isolated from MCF-7 cells using Trizol (Invitrogen), according to the manufacturer's instructions. The qPCR assays were conducted with the aid of a QuantiTect SYBR Green RT-PCR Kit (Qiagen) and an ABI PRISM 7900HT sequence detection system (Applied Biosystems). The relative changes in transcript levels for each sample were determined by normalizing to glyceraldehyde 3-phosphate dehydrogenase mRNA levels. Primer sequences used for qPCR analysis are shown in Supplementary Table 2.

Reverse transcription PCR analysis of S1PRs. Total RNA was isolated from MCF-7 cells using Trizol, according to the manufacturer's instructions. A SuperScript III Fast-Strand Synthesis System (Invitrogen) was used for reverse transcription synthesis of cDNAs. PCR amplification was performed with PrimeStar HS DNA polymerase (Takara) using GeneAmp PCR System 9700 (Applied

Biosystems). The cycling conditions were as follows: 1 min at 95 °C, 40 cycles of 30 s at 95 °C, 30 s at 54–66 °C, 1 min at 72 °C, following 7 min at 72 °C. Primer sequences used for reverse transcription PCR analysis are shown in Supplementary Table 2.

Transient RNA interference. Double-strand RNA oligonucleotides (siRNAs) against *S1PR3*, *S1PR2* and appropriate control scrambled siRNA were from Santa Cruz Biotechnology. The siRNAs against *Notch1*, *ABCC1* and *Spns2* were from Invitrogen. The siRNAs were transfected into MCF-7 cells using RNAiMax (Invitrogen) according to the manufacturer's recommendations.

Stable knockdown by lentiviral shRNA transduction. For stable gene silencing of *S1PR3* or *S1PR2*, specific shRNA MISSION lentiviruses (Sigma-Aldrich) were transduced into cells. The target sequence was 5′-CCGGGATCCTCTACGCAC GCATCTACTCGAGTAGATGCGTGCGTAGAGGATCTTTTTG-3′ for sh*S1PR3* and 5′-CCGGACTTTACCACCTGGTACAAAGCTCGAGCTTTGTACCAGGTG GTAAAGTTTTTTG-3′ for sh*S1PR2*. The transduced cells were selected in growth medium containing 1.5 μg ml^{-1} puromycin (Sigma-Aldrich).

Immunoblot analysis. Cells were lysed in Cell Lysis Buffer (Cell Signaling Technology) on ice for 30 min. Lysates were subjected to sodium dodecyl sulphate polyacrylamide gel electrophoresis and transferred to Immobilon-P Transfer Membrane (Millipore). Membranes were blocked with 5% (w/v) bovine serum albumin in Tris-buffered saline containing 0.1% Tween-20 (TBST) and incubated with primary antibodies overnight at 4 °C. Membranes were then incubated with horseradish peroxidase-conjugated secondary antibodies (Cell Signaling Technology, 1:2,000) for 1 h at room temperature and detected using ECL Prime Western Blotting Detection Reagent (GE Healthcare). Images were acquired using a LAS-3000 Imager (Fujifilm). The density of each band was quantified using an image analyser (Multi Gauge software, Fujifilm). The primary antibodies used were S1PR3 (#sc-30024, 1:2,000), S1PR2 (#sc-25491, 1:1,000), Notch1 (#4380, 1:1,000), N1ICD (#2421, 1:1,000), Notch3 (#2889, 1:1,000), FLAG (#F1804, 1:1,000), myc (#C3956, 1:5,000), HA (#H6908, 1:1,000), phospho-ADAM17 (#SAB4504073, 1:1,000), ADAM17 (#AB19027, 1:1,000), phospho-p38MAPK (#9211, 1:1,000), p38MAPK (#9212, 1:1,000), phospho-Akt (#9271, 1:1,000), Akt (#9272, 1:1,000), SphK1 (#AP7237c, 1:500), SphK2 (a gift from Dr T. Okada at Kobe University, 1:3,000), ABCC1 (#ab3368, 1:1,000), Spns2 (#sc-130102, 1:1,000) and β-actin (#A5441, 1:10,000). Original immunoblots are shown in Supplementary Fig. 19.

Immunocytochemistry. SphK-overexpressing MCF-7 cells and mammosphere cells were plated on glass coverslips. Cells were fixed with 4% paraformaldehyde and permeabilized with 0.2% Triton X-100. Coverslips were blocked with 5% FBS and incubated overnight at 4 °C with primary antibodies that recognized FLAG (#F1804, 1:500), HA (#H6908, 1:120), SphK1 (#ab46719, 1:50), S1PR3 (#sc-30024, 1:50), ALDH1 (#611194, 1:100). ADAM17 (#ab57484, 1:300) and activated Notch1 (#ab8925, 1:200). After rinsing with PBS, coverslips were incubated for 1 h at room temperature with Alexa488-conjugated (#A11034, 1:200) or Alexa555-conjugated (#A21424, 1:200) secondary antibody. In the case of triple staining of Sphk1, ALDH1 and N1ICD, antibody to SphK1 was labelled with AMCA conjugation kit (Abcam). After rinsing with PBS, coverslips were incubated with AMCA-conjugated SphK1 antibody (1:100) for 1.5 h. Nuclei were counterstained with DAPI (Nacalai Tesque). Fluorescence images were obtained using a Nikon A1 confocal microscope (Nikon).

Immunoprecipitation assay. Immunoprecipitation was conducted as previously reported with slight modifications[51]. MCF-7 cells were transfected with myc-tagged ADAM17. At 48 h after transfection, cells were lysed in lysis buffer (20 mM Tris–HCl pH 7.4, 200 mM NaCl, 0.1% NP-40, 10 mM NaF, 1 mM Na_3VO_4 and complete mini protease inhibitor cocktail (Roche Applied Sciences)). Lysates (100 μg) were incubated with myc-specific polyclonal antibody (#C3956, 1 μg) or normal rabbit IgG (#PM035, MBL, 1 μg) overnight at 4 °C. Subsequently, Protein G Sepharose (Amersham Pharmacia Biotech) was added to the mixture and incubated for an additional 2 h at 4 °C. Beads were washed with lysis buffer and immunoprecipitated proteins analysed by immunoblotting using a p38MAPK-specific polyclonal antibody (#9212) and a myc-specific polyclonal antibody (#C3956).

ADAM17 activity. ADAM17 activity was measured using a SensoLyte 520 ADAM17 Activity Assay Kit (ANASPEC) according to the manufacture's instruction[52]. MCF-7 cells were scraped in PBS containing a complete mini protease inhibitor cocktail and lysed using five cycles of freeze–thawing. Lysed cells were centrifuged at 20,000 *g* for 15 min and pelleted membranes resuspended with assay buffer. Approximately 15 μg of proteins were mixed with substrate for 30 min and fluorescence intensity was measured using a Wallac1420ARVO fluoroscan (Perkin Elmer), with excitation at 490 nm and emission at 520 nm.

γ-secretase activity. The activity of γ-secretase was measured using a specific fluorogenic substrate assay[53]. Cells were collected in cell lysis buffer containing (20 mM HEPES pH 7.0, 150 mM KCl, 2 mM EDTA, 1% (3-cholamidopropyl) dimethylammonio]-2-hydroxy-1-propanesulfonate (CHAPSO; Dojindo Laboratories), and complete Mini, EDTA-free protease inhibitor cocktail (Roche)). Lysates were centrifuged at 10,000 *g* for 1 min at 4 °C to remove nuclei and large cell debris. Approximately 5 μg of protein was added to each well of a white 96-well polystyrene microplate (Packard) and an equal volume of assay buffer (50 mM Tris–HCl (pH 6.8), 2 mM EDTA, and 0.25% (3-cholamidopropyl) dimethylammonio]-2-hydroxy-1-propanesulfonate (w/v)) added. 10 μM fluorogenic γ-secretase substrate (Peptide) was added to the plate and samples incubated at 37 °C for 4 h in the dark. Fluorescence intensity was measured using a Wallac1420ARVO fluoroscan (Perkin Elmer) with excitation at 355 nm and emission at 460 nm.

SphK activity. SphK activity was measured using omega-(7-nitro-2-1,3-benzoxadiazol-4-yl)-D-erythro-sphingosine-labelled fluorescent substrate[54]. Cells were lysed with a single freeze–thaw cycle in 50 mM HEPES (pH 7.4), 10 mM KCl, 15 mM $MgCl_2$, 0.1% Triton X-100, 20% glycerol, 2 mM orthovanadate, 2 mM dithiothreitol, 10 mM NaF, 1 mM deoxypyridoxine and complete Mini, EDTA-free protease inhibitor cocktail (Roche). The lysate was cleared by centrifuging at 20,000 *g* for 15 min at 4 °C. SphK1 activity was measured in 50 mM HEPES (pH 7.4), 15 mM $MgCl_2$, 0.5% Triton X-100, 10% glycerol, 5 mM NaF, 1 mM deoxypyridoxine, 2 mM ATP and 10 μM NBD-sphingosine (Avanti Polar Lipids). SphK2 activity was measured in 50 mM HEPES (pH 7.4), 15 mM $MgCl_2$, 0.5 M KCl, 10% glycerol, 5 mM NaF, 1 mM deoxypyridoxine, 2 mM ATP and 10 μM NBD- sphingosine. Reactions were started with the addition of 5 μg of lysate protein and incubated for 4 h at room temperature. Reactions were extracted with the addition of 1 M potassium phosphate (pH 8.5), followed by chloroform/methanol (2:1), then cleared at 15,000 *g* for 1 min. The upper aqueous layer was placed into the wells of white 96-well polystyrene microplates (Packard). Fluorescence intensity was measured with a Wallac1420ARVO fluoroscan (Perkin Elmer) with excitation at 485 nm and emission at 535 nm.

Tumorigenicity assay. The animal study protocol was reviewed and approved by the animal care and use committee of the institute. Six-week-old female Balb/c nude mice (CLEA Japan) were used in these studies and were given injections of 17-β-estradiol (Sigma-Aldrich) dissolved in pure sesame oil (0.1 mg 0.05 ml^{-1} sesame oil per mouse, subcutaneously) 1 day before tumour inoculation, and at weekly intervals, according to a previously reported protocol with slight modifications[55]. The ALDH-positive cell population was sorted by FACS (BD Aria II) and suspended in PBS mixed with an equal volume of Matrigel (BD Biosciences). Mice were given bilateral subcutaneous injections of 1×10^5 (0.1 ml) cells. Tumour growth was monitored for 6 weeks and analysed. Tumour volume was determined using the formula: $V = ½ \times$ larger diameter $\times$ (smaller diameter)^2.

For the immunohistochemistry, paraffin-embedded sections of breast tumours from xenografts were deparaffinized in xylene and rehydrated in graded alcohol. Antigen retrieval was conducted three times by microwaving the slides in 0.01 M citrate buffer (pH 6.0) for 5 min. Sections were blocked with 5% FBS and incubated for 1.5 h with primary antibodies that recognized S1PR3 (#sc-30024, 1:50) and ALDH1 (#611194, 1:100). After rinsing with PBS, coverslips were incubated for 1 h at room temperature with Alexa488-conjugated (#A11034, 1:200) or Alexa555-conjugated (#A21424, 1:200) secondary antibody. Nuclei were counterstained with DAPI (Nacalai Tesque). Fluorescence images were obtained using a Biorevo BZ-9000 (Keyence). The number of S1PR3- and ALDH1 double-positive cells was counted in five fields[56].

For the hierarchy assay, the xenografts were collected after 6 weeks, dissociated into single cells and TRA-1-85-positive cells analysed using the ALDH assays[57]. Single cells were suspended in ALDH assay buffer containing the BAAA (1 μM) and incubated 30 min at 37 °C. The cells were resuspended in ALDH assay buffer for subsequent staining with the APC-conjugated TRA-1-85 antibody (#FAB3195A, 1:10), which recognizes human cells and thereby allows their discrimination from mouse cells. After incubation for 30 min and following centrifugation, the cells were resuspended in ALDH assay buffer containing 7-AAD (BD Bioscience, #559925) and analysed with a FACS Aria II cell sorter (BD Bioscience).

For the chronic administration, TY52156 (167 mg ml^{-1} in a 1:1 mixture of DMSO and PEG400) was inserted in subcutaneously implanted Alzet osmotic pumps (Cupertino), designed to release TY52156 continuously (at about 25 μg h^{-1}) for 6 weeks.

Mammosphere formation from primary cells. Mammosphere formation using primary cells (Celprogen) was performed[7,8]. The cells were plated as single cells in ultralow attachment dishes (Corning) at a density of 20,000 viable cells ml^{-1} in mammary epithelial growth medium for 7 days. To make secondary mammospheres, primary mammospheres were collected by gentle centrifugation (200*g*), dissociated enzymatically (10 min in 0.05% trypsin–EDTA) and mechanically (pipetting with yellow tips) into a single-cell suspension. The cells obtained from dissociation were then seeded in ultralow attachment dishes in mammary epithelial growth medium again.

Statistical analysis. Results are shown as mean ± s.d. For tumour incidence, the *P* value was calculated using the Fisher's exact test (Fig. 6a,g,h). Bonferroni correction was applied for multiple comparisons (Fig. 6a,g). For tumour volume, the *P* value was calculated using the Kruskal–Wallis test, followed by *post hoc* Steel–Dwass's multiple comparison test (Fig. 6c). Differences at $P<0.05$ were considered to be significant. Statistical analyses were performed using Excel 2010 with the add-in software.

References

1. Visvader, J. E. & Lindeman, G. J. Cancer stem cells in solid tumours: accumulating evidence and unresolved questions. *Nat. Rev. Cancer* **8,** 755–768 (2008).
2. Bonnet, D. & Dick, J. E. Human acute myeloid leukemia is organized as a hierarchy that originates from a primitive hematopoietic cell. *Nat. Med.* **3,** 730–737 (1997).
3. Al-Hajj, M. *et al.* Prospective identification of tumorigenic breast cancer cells. *Proc. Natl Acad. Sci. USA* **100,** 3983–3988 (2003).
4. Ginestier, C. *et al.* ALDH1 is a marker of normal and malignant human mammary stem cells and a predictor of poor clinical outcome. *Cell Stem Cell* **1,** 555–567 (2007).
5. Jiang, F. *et al.* Aldehyde dehydrogenase 1 is a tumour stem cell-associated marker in lung cancer. *Mol. Cancer Res.* **7,** 330–338 (2009).
6. van den Hogen, C. *et al.* High aldehyde dehydrogenase activity identifies tumour-initiating and metastasis-initiating cells in human prostate cancer. *Cancer Res.* **70,** 5163–5173 (2010).
7. Hinohara, K. *et al.* ErbB receptor tyrosine kinase/NF-κB signaling controls mammosphere formation in human breast cancer. *Proc. Natl Acad. Sci. USA* **109,** 6584–6589 (2012).
8. Dontu, G. *et al. In vitro* propagation and transcriptional profiling of human mammary stem/progenitor cells. *Genes Dev.* **17,** 1253–1270 (2003).
9. Takebe, N. & Ivy, S. P. Controversies in cancer stem cells: targeting embryonic signaling pathways. *Clin. Cancer Res.* **16,** 3106–3112 (2010).
10. Scheel, C. *et al.* Paracrine and autocrine signals induce and maintain mesenchymal and stem cell states in the breast. *Cell* **145,** 926–940 (2011).
11. Takabe, K., Paugh, S. W., Milstian, S. & Spiegel, S. 'Inside-out' signalling of sphingosine-1-phosphate: therapeutic targets. *Pharmacol. Rev.* **60,** 181–195 (2008).
12. Kohama, T. *et al.* Molecular cloning and functional characterization of murine sphingosine kinase. *J. Biol. Chem.* **273,** 23722–23728 (1998).
13. Liu, H. *et al.* Molecular cloning and functional characterization of a novel mammalian sphingosine kinase type 2 isoform. *J. Biol. Chem.* **275,** 19513–19520 (2000).
14. Pyne, N. J. & Pyne, S. Sphingosine 1 phosphate and cancer. *Nat. Rev. Cancer* **10,** 489–503 (2010).
15. Fyrst, H. & Saba, J. D. An update on sphingosine-1-phosphate and other sphingolipid mediators. *Nat. Chem. Biol.* **6,** 489–497 (2010).
16. Nagahashi, M. *et al.* Sphingosine-1-phosphate produced by sphingosine kinase 1 promotes breast cancer progression by stimulating angiogenesis and lymphangiogenesis. *Cancer Res.* **72,** 726–735 (2012).
17. Charafe-Jauffret, E. *et al.* Breast cancer cell lines contain functional cancer stem cells with metastatic capacity and a distinct molecular signature. *Cancer Res.* **69,** 1302–1313 (2009).
18. Hirata, N., Sekino, Y. & Kanda, Y. Nicotine increases cancer stem cell population in MCF-7 cells. *Biochem. Biophys. Res. Commun.* **403,** 138–143 (2010).
19. Long, J. S. *et al.* Sphingosine 1-phosphate receptor 4 uses HER2 (ERBB2) to regulate extracellular signal regulated kinase-1/2 in MDA-MB-453 breast cancer cells. *J. Biol. Chem.* **285,** 35957–35966 (2010).
20. Lin, C. I., Chen, C. N., Lin, P. W. & Lee, H. Sphingosine-1-phosphate regulates inflammation-related genes in human endothelial cells thorough S1P1 and S1P3. *Biochem. Biophys. Res. Commun.* **355,** 895–901 (2007).
21. Murakami, A. *et al.* Sphingosine 1-phosphate (S1P) regulates vascular contraction via S1P3 receptor: investigation based on a new S1P3 receptor antagonist. *Mol. Pharmacol.* **77,** 704–713 (2010).
22. Pannuti, A. *et al.* Targeting Notch to target cancer stem cells. *Clin. Cancer Res.* **16,** 3141–3152 (2010).
23. Noseda, M. *et al.* Smooth muscle α-actin is a direct target of Notch/CSL. *Circ. Res.* **98,** 1468–1470 (2006).
24. Jefflies, S., Robins, D. J. & Capobianco, A. J. Characterization of a high-molecular-weight Notch complex in the nucleus of Notch^{ic}-transformed RKE cells and in a human T-cell leukemia cell line. *Mol. Cell. Biol.* **22,** 3927–3941 (2002).
25. Artavanis-Tsakonas, S. & Muskavitch, M. A. Notch: the past, the present, and the future. *Curr. Top. Dev. Biol.* **92,** 1–29 (2010).
26. Ladi, E. *et al.* The divergent DSL ligand Dll3 does not activate Notch signaling but cell autonomously attenuates signaling induced by other DSL ligands. *J. Cell Biol.* **170,** 983–992 (2005).
27. Liu, C. *et al.* TACE-mediated ectodomain shedding of the type I TGF-β receptor downregulates TGF-β signaling. *Mol. Cell* **35,** 25–36 (2009).
28. Lammich, S. *et al.* Constitutive and regulated α-secretase cleavage of Alzheimer's amyloid precursor protein by a disintegrin metalloprotease. *Proc. Natl Acad. Sci. USA* **96,** 3922–3927 (1999).
29. Diaz-Rodriguez, E. *et al.* Extracellular signal-regulated kinase phosphorylates tumour necrosis factor alpha-converting enzyme at threonine 735: a potential role in regulated shedding. *Mol. Biol. Cell* **13,** 2031–2044 (2002).
30. Fan, H., Turck, C. W. & Derynck, R. Characterization of growth factor-induced serine phosphorylation of tumour necrosis factor-alpha converting enzyme and of an alternatively translated polypeptide. *J. Biol. Chem.* **278,** 18617–18627 (2003).
31. Xu, P. & Derynck, R. Direct activation of TACE-mediated ectodomain shedding by p38 MAP kinase regulates EGF receptor-dependent cell proliferation. *Mol. Cell* **37,** 551–566 (2010).
32. Pitson, S. M. *et al.* Phosphorylation-dependent translocation of sphingosine kinase to the plasma membrane drives its oncogenic signaling. *J. Exp. Med.* **201,** 49–54 (2005).
33. Igarashi, N. *et al.* Sphingosine kinase 2 is a nuclear protein and inhibits DNA synthesis. *J. Biol. Chem.* **278,** 46832–46839 (2003).
34. Takabe, K. *et al.* Estradiol induces export of sphingosine 1-phosphate from breast cancer cells via ABCC1 and ABCG2. *J. Biol. Chem.* **285,** 10477–10486 (2010).
35. Kawahara, A. *et al.* The sphingolipid transporter spns2 functions in migration of zebrafish myocardial precursors. *Science* **323,** 524–527 (2009).
36. Pébay, A. *et al.* Essential roles of sphingosine-1-phosphate and platelet-derived growth factor in the maintenance of human embryonic stem cells. *Stem Cells* **23,** 1541–1548 (2005).
37. Pitson, S. M. & Pébay, A. Regulation of stem cell pluripotency and neural differentiation by lysophospholipids. *Neurosignals* **17,** 242–254 (2009).
38. Bozkulak, E. C. & Weinmaster, G. Selective use of ADAM10 and ADAM17 in activation of Notch1 signaling. *Mol. Cell. Biol.* **29,** 5679–5695 (2009).
39. van Tetering, G. *et al.* Metalloprotease ADAM10 is required for Notch1 site 2 cleavage. *J. Biol. Chem.* **284,** 31018–31027 (2009).
40. Lu, J. *et al.* Endothelial cells promote the colorectal cancer stem cell phenotype through a soluble form of Jagged-1. *Cancer Cell* **23,** 171–185 (2013).
41. Inoue, A. *et al.* TGFα shedding assay: an accurate and versatile method for detecting GPCR activation. *Nat. Methods* **9,** 1021–1029 (2012).
42. Harrison, H. *et al.* Regulation of breast cancer stem cell activity by signaling through the Notch 4 receptor. *Cancer Res.* **70,** 709–718 (2010).
43. Ruckhäberle, E. *et al.* Microarray analysis of altered sphingolipid metabolism reveals prognostic significance of sphingosine kinase 1 in breast cancer. *Breast Cancer Res. Treat.* **112,** 41–52 (2008).
44. Watson, C. *et al.* High expression of sphingosine 1-phosphate receptors, S1P1 and S1P3, sphingosine kinase 1, and extracellular signal-regulated kinase-1/2 is associated with development of tamoxifen resistance in estrogen receptor-positive breast cancer patients. *Am. J. Pathol.* **177,** 2205–2215 (2010).
45. Long, J. S. *et al.* Sphingosine kinase 1 induces tolerance to human epidermal growth factor receptor 2 and prevents formation of a migratory phenotype in response to sphingosine 1-phosphate in estrogen receptor-positive breast cancer cells. *Mol. Cell. Biol.* **30,** 3827–3841 (2010).
46. Goetzl, E. J. *et al.* Dual mechanisms for lysophospholipid induction of proliferation of human breast carcinoma cells. *Cancer Res.* **59,** 4732–4737 (1999).
47. Ranganathan, P., Weaver, K. L. & Capobianco, A. J. Notch signaling in solid tumours: a little bit of everything but not all the time. *Nat. Rev. Cancer* **11,** 338–351 (2011).
48. Debeb, B. G. *et al.* Pre-clinical studies of Notch signaling inhibitor RO4929097 in inflammatory breast cancer cells. *Breast Cancer Res. Treat.* **134,** 495–510 (2012).
49. Ramakrishnan, V. *et al.* MRK003, a γ-secretase inhibitor exhibits promising *in vitro* pre-clinical activity in multiple myeloma and non-Hodgkin's lymphoma. *Leukemia* **26,** 340–348 (2012).
50. Olsauskas-Kuprys, R., Zlobin, A. & Osipo, C. Gamma secretase inhibitors of Notch signaling. *OncoTargets Ther.* **6,** 943–955 (2013).
51. Kanda, Y., Mizuno, K., Kuroki, Y. & Watanabe, Y. Thrombin-induced p38 mitogen-activated protein kinase activation is mediated by epidermal growth factor receptor transactivation pathway. *Br. J. Pharmacol.* **132,** 1657–1664 (2001).
52. Rao, S., Liu, X., Freedman, B. D. & Behrens, E. M. Spleen tyrosine kinase (Syk)-dependent calcium signals mediate efficient CpG-induced exocytosis of tumour necrosis factor α (TNFα) in innate immune cells. *J. Biol. Chem.* **288,** 12448–12458 (2013).
53. Farmery, M. R. *et al.* Partial purification and characterization of gamma-secretase from post-mortem human brain. *J. Biol. Chem.* **278,** 24277–24284 (2003).

54. Don, A. S. *et al.* Essential requirement for sphingosine kinase 2 in a sphongolipid apoptosis pathway activated by FTY720 analogues. *J. Biol. Chem.* **282,** 15833–15842 (2007).
55. Zhou, J. *et al.* Activation of the PTEN/mTOR/STAT3 pathway in breast cancer stem-like cells is required for viability and maintenance. *Proc. Natl Acad. Sci. USA* **104,** 16158–16163 (2007).
56. Ahn, G. & Brown, J. M. Matrix metalloproteinase-9 is required for tumour vasculogenesis but not for angiogenesis: role of bone marrow-derived myelomonocytic cells. *Cancer Cell* **13,** 193–205 (2008).
57. Prasmickaite, L. *et al.* Aldehyde dehydrogenase (ALDH) activity does not select for cells with enhanced aggressive properties in malignant melanoma. *PLoS ONE* **5,** e10731 (2010).

Acknowledgements

We thank Dr Taro Okada for his helpful comments on the manuscript. We thank Stuart M. Pitson (University of Adelaide), Taro Okada (Kobe University), Aly Karsan (British Columbia Cancer Research Centre), Anthony J. Capobianco (University of Pennsylvania), Spyros Artavanis-Tsakonas (Harvard Medical School), Stefan Lichtenthaler (Ludvig Maximilians University), Lothar J. Strobl (German Research Center for Environmental Health), Michael J. Hendzel (University of Alberta), Rik Derynck (University of California, San Francisco), and J. Silvio Gutkind (National Institutes of Health) for providing the plasmids. We thank Dr Junya Kanda (Jichi Medical University) for assistance with statistical analyses. We also thank additional members of the laboratory and other members of the Institute for their advice and discussion. This work was supported by the Advanced research for medical products Mining Programme of the National Institute of Biomedical Innovation (NIBIO, #09-02 to Y.K.), a Grant-in-Aid for Scientific Research from the Ministry of Education, Culture, Sports, Science, and Technology, Japan (#23590322, #26670041 to Y.K.), a Health and Labour Sciences Research Grant from the Ministry of Health, Labour and Welfare, Japan (Y.K.), and a grant from the Smoking Research Foundation (Y.K.).

Author contributions

N.H. performed most of the experiments. Y.K. planned the project. Y.K. and Y.S. wrote the manuscript. S.Y. performed the experiments related to ADAM17 mutants. T.S. and M.K. performed the experiments related to TY52156. All authors participated in the preparation of the manuscript.

Additional information

Accession codes: Microarray data have been deposited in the NCBI Gene Expression Omnibus database under accession codes GSE59653.

Supplementary Information accompanies this paper at http://www.nature.com/naturecommunications

Competing financial interests: The authors declare no competing financial interests.

Reprints and permission information is available online at http://npg.nature.com/reprintsandpermissions/

How to cite this article: Hirata, N. *et al.* Sphingosine-1 phosphate promotes expansion of cancer stem cells via S1PR3 by a ligand-independent Notch activation. *Nat. Commun.* 5:4806 doi: 10.1038/ncomms5806 (2014).

Journal of Neurochemistry JNC

JOURNAL OF NEUROCHEMISTRY | 2014 | 128 | 507–522 doi: 10.1111/jnc.12486

ORIGINAL ARTICLE

Spikar, a novel drebrin-binding protein, regulates the formation and stabilization of dendritic spines

Hiroyuki Yamazaki,* Nobuhiko Kojima,* Kenichi Kato,* Eiji Hirose,† Toshiharu Iwasaki,‡ Toshiyuki Mizui,* Hideto Takahashi,*,[1] Kenji Hanamura,* Reiko T. Roppongi,* Noriyuki Koibuchi,‡ Yuko Sekino,*,§ Nozomu Mori†,[2] and Tomoaki Shirao*

*Department of Neurobiology and Behavior, Gunma University Graduate School of Medicine, Maebashi, Japan

†National Center for Geriatrics and Gerontology, Obu, Japan

‡Integrative Physiology, Gunma University Graduate School of Medicine, Maebashi, Japan

§Division of Pharmacology, National Institute of Health Sciences, Tokyo, Japan

Abstract

Dendritic spines are small, actin-rich protrusions on dendrites, the development of which is fundamental for the formation of neural circuits. The actin cytoskeleton is central to dendritic spine morphogenesis. Drebrin is an actin-binding protein that is thought to initiate spine formation through a unique drebrin-actin complex at postsynaptic sites. However drebrin overexpression in neurons does not increase the final density of dendritic spines. In this study, we have identified and characterized a novel drebrin-binding protein, spikar. Spikar is localized in cell nuclei and dendritic spines, and accumulation of spikar in dendritic spines directly correlates with spine density. A reporter gene assay demonstrated that spikar acts as a transcriptional co-activator for nuclear receptors. We found that dendritic spine, but not nuclear, localization of spikar requires drebrin. RNA-interference knockdown and overexpression experiments demonstrated that extranuclear spikar regulates dendritic spine density by modulating *de novo* spine formation and retraction of existing spines. Unlike drebrin, spikar does not affect either the morphology or function of dendritic spines. These findings indicate that drebrin-mediated postsynaptic accumulation of spikar regulates spine density, but is not involved in regulation of spine morphology.

Keywords: dendritic spine, drebrin-binding protein, spine formation, transcriptional co-activator.

J. Neurochem. (2014) **128**, 507–522.

*Read the **Editorial Highlight** for this article on page 473.*

Neurons have numerous small, actin-rich protrusions called dendritic spines that receive the majority of excitatory inputs (Sala *et al.* 2008; Rochefort and Konnerth 2012). The formation of dendritic spines plays a pivotal role in the incorporation of neurons into neural circuits (Kwon and Sabatini 2011). It is widely accepted that dendritic filopodia are the precursors of dendritic spines and that the actin cytoskeleton is a central player in the morphological changes underlying dendritic spine formation (Ethell and Pasquale 2005; Sekino *et al.* 2007; Shirao and Gonzalez-Billault 2013).

Drebrin is an actin-binding protein that has been extensively studied. Drebrin bridges two actin protomers (Grintsevich *et al.* 2010) and induces structural and

Received July 25, 2013; revised manuscript received October 9, 2013; accepted October 10, 2013.

Address correspondence and reprint requests to Tomoaki Shirao, Department of Neurobiology and Behavior, Gunma University Graduate School of Medicine, 3-39-22 Showa-machi, Maebashi 371-8511, Japan. E-mail: tshirao@med.gunma-u.ac.jp.

[1]Present address: Institut de recherches cliniques de Montreal, Montreal, QC, Canada, H2W 1R7. [2]Present address: Department of Anatomy and Neurobiology, Nagasaki University School of Medicine, Nagasaki, Nagasaki 852-8523, Japan.

Abbreviations used: ADF-H domain, actin-depolymerizing factor homology domain; BSA, bovine serum albumin; DIV, days *in vitro*; DMEM, Dulbecco's modified Eagle medium; drebrinR, RNAi-resistant drebrin; ERα, estrogen receptor α; GR, glucocorticoid receptor; His^6-drebrin, His^6-tagged drebrin A; KD, knockdown; LUC, luciferase; mDsRED, monomeric DsRED; MEM, minimum essential medium; mEPSCs, miniature excitatory postsynaptic currents; mNLS, mutated NLS; NLS, nuclear localization sequence; PBS, phosphate-buffered saline; RNAi, RNA interference; $spikar^R$, RNAi-resistant spikar; T3, 3,3′,5-triiodo-L-thyronine; TRE, thyroid hormone response element; TRβ1, thyroid hormone receptor β1.

mechanical remodeling of *F*-actin that includes significant changes in filament helical twisting and stiffness (Sharma *et al.* 2011, 2012). Within cultured cells, overexpressed drebrin binds to *F*-actin (Shirao *et al.* 1988; Ishikawa *et al.* 1994) to form unique *F*-actin bundles that are different from those observed in stress fibers or lamellipodia (Shirao *et al.* 1994). Formation of a drebrin-actin complex at postsynaptic sites during development facilitates dendritic spine formation (Takahashi *et al.* 2003; Aoki *et al.* 2005). Drebrin knockdown decreases spine and filopodia densities (Takahashi *et al.* 2006) and the density of excitatory synapses (Ivanov *et al.* 2009). However, drebrin overexpression does not increase the number of normal spines (Hayashi and Shirao 1999; Mizui *et al.* 2005), even though it causes morphological changes in dendritic spines (Hayashi and Shirao 1999; Biou *et al.* 2008). These results indicate that drebrin initiates spine formation, but an increased amount of drebrin does not directly correlate with the final density of dendritic spines.

We postulated the existence of a novel drebrin-binding protein that plays a critical role in regulating spine density through changes in its expression level. Although drebrin forms a complex with actin, myosin, and gelsolin (Hayashi *et al.* 1996) as well as other drebrin-binding proteins such as Homer2 (Shiraishi *et al.* 2004) and profilin (Mammoto *et al.* 1998), spine density does not vary in direct proportion to the expression level of these molecules (Sala *et al.* 2003; Ryu *et al.* 2006; Gorlich *et al.* 2012). To identify a drebrin-binding molecule directly related to spine density, we performed a yeast two-hybrid screen using drebrin as bait. Based on the screen results, we isolated a novel drebrin-binding protein that we termed spikar (for **spi**ne and **kar**yoplasm protein). Knockdown and overexpression experiments performed with spikar indicated that its expression level parallels the density of dendritic spines.

Methods

Animals

All experiments were carried out in accordance with the guidelines of the Animal Care and Experimentation Committee, Gunma University, Showa Campus (Maebashi, Japan). Wistar rats were purchased from Japan SLC Inc. (Hamamatsu, Japan) and Charles River Laboratories Japan Inc. (Yokohama, Japan). Every effort was made to minimize animal suffering and reduce the number of animals used. Animals were kept in the animal house under standard white cyclic lighting, with free access to food and water.

Yeast two-hybrid system

The *Saccharomyces cerevisiae* transformation and two-hybrid screen were carried out using the Y190 strain. The N-terminal region of rat drebrin (corresponding to amino acid residues 1–233) was subcloned into the pAS404 vector, which was derived from pAS1 (Sekiguchi *et al.* 2001). Y190 cells were transformed with the bait plasmid pAS404-drebrin (1–233), using the conventional lithium acetate-polyethylene glycol method. The cells were grown on SD medium lacking tryptophan and further characterized by testing for protein expression and self-activation of the bait before screening. Large-scale transformation was performed using a rat brain cDNA library constructed in a pACT2 vector (Clontech, Palo Alto, CA, USA), and the cells were grown on SD medium lacking tryptophan, leucine, and histidine, and containing 25 mM 3-aminotriazole. The cells were subsequently assayed for activation of the HIS3 genes.

Molecular cloning of spikar cDNA

The rat spikar clone isolated from the two-hybrid screen lacked a 5′-coding sequence; therefore, the full-length cDNA was generated using a PCR-based strategy. To obtain the 5′ end of rat spikar cDNA, we performed 5′-rapid amplification of cDNA ends (RACE) using rat hippocampal cDNA and a 5′-Full RACE Core Set (Takara, Otsu, Japan).

Expression vectors

All spikar and drebrin constructs were generated by PCR using Pfu turbo DNA polymerase (Stratagene, La Jolla, CA, USA). Full-length spikar and its deletion mutants were subcloned into pEGFP-C1 (EGFP, enhanced green fluorescent protein) (Clontech), pCMV-Myc (Clontech) or pNN265-HA (Kojima *et al.* 1997). To generate the nuclear localization signal (NLS) mutant of spikar (mNLS-spikar), K44T and K45T mutations were introduced by PCR using the following primers: 5′-gccccattaaaacgacaaagaaacccggc-3′ and 5′-gccgggtttctttgtcgttttaatggggc-3′.monomeric DsRED-drebrin A was constructed by subcloning a rat drebrin A fragment into the pDsRed-Monomer-C1 (Clontech).

Reporter gene assays

The method of reporter gene assay has been described previously (Takeshita *et al.* 1998; Iwasaki *et al.* 2001, 2002). The details are provided in the Appendix S1.

In vitro binding assay

A binding assay for full-length drebrin and full-length spikar was performed using green fluorescent protein (GFP)-spikar and His^6-tagged drebrin A (His^6-drebrin). The His^6-drebrin construct was a gift from Dr Ishikawa (Ishikawa *et al.* 2007). His^6-drebrin was affinity purified using Ni-NTA Magnetic Agarose Beads (Qiagen, Hilden, Germany). Ni-NTA beads conjugated with His^6-drebrin were incubated with cell lysate expressing GFP-spikar for 2 h at 25°C. Following extensive washes with lysis buffer (20 mM Tris-HCl, pH 7.5, 150 mM NaCl, 1% NP40, 50 μg/mL DNase, 10 μg/mL RNase, 1 mM phenylmethanesulfonyl fluoride, 1 μg/mL leupeptin, and 1 μg/mL pepstatin), the Ni-NTA bead pellets were re-suspended in sodium dodecyl sulfate (SDS) sample buffer and analyzed by western blotting. For GST pull-down assay, Glutathione S-transferase (GST)-drebrin (1–138) (pGEX-4T-1, GE Health Care, Buckinghamshire, England) was purified directly from bacterial extracts on glutathione-Sepharose-4B (GE Health Care). Immobilized GST or GST-drebrin (1–138) fusion proteins were incubated with cell lysate expressing HA-spikar fragments (1–376, 377–1208, or 1–1208) for 2 h at 25°C. After extensive washes with lysis buffer, the GST bead pellets were re-suspended in SDS sample buffer and analyzed by western blotting.

Immunocytochemistry and immunohistochemistry

Cultured neurons were fixed in 4% paraformaldehyde at 4°C for 20 min. The fixed neurons were permeabilized with 0.1% Triton X-100 in phosphate-buffered saline (PBS) for 5 min and blocked with 3% bovine serum albumin (BSA) in PBS for 60 min. Primary antibodies were applied in 3% BSA/PBS at 4°C for 12 h. After washing with PBS three times for 5 min each, the appropriate secondary antibodies conjugated to fluorescein isothiocyanate, Cy5, or rhodamine (Chemicon, Temecula, CA, USA) were added and incubated for 1 h at 20–25°C.

Deeply anesthetized 7-week-old male Wistar rats were perfused intracardially with a fixative of 4% paraformaldehyde in 0.1 M phosphate buffer (pH 7.4). Brain tissue was post-fixed in the same fixative for 12 h and then equilibrated with 30% sucrose in PBS at 4°C. Frozen sections (25 μm) were cut on a cryostat and treated with 0.1% Triton X-100 in PBS for 10 min and then incubated with 3% BSA/PBS for 1 h. They were then incubated with the primary antibody for 12 h at 4°C, washed with PBS four times for 5 min each, incubated with a biotinylated secondary antibody (Vector Laboratories, Burlingame, CA, USA) for 1 h at 20–25°C, and washed four times for 5 min each. Visualization was performed with 3,3′-diaminobenzidine using the ABC method (Vectastain Elite kit, Vector Laboratories).

Western blot analysis and subcellular fractionation

Wistar rats were sacrificed after being deeply anesthetized, and various tissues were dissected and homogenized. Protein amounts were normalized to the wet weights of the original tissue samples. For subcellular fractionation, the cerebral cortices of seven adult male Wistar rats were homogenized in a buffered solution (320 mM sucrose, 4 mM HEPES-NaOH, pH 7.4) containing a protease inhibitor cocktail (Complete, Roche, Basel, Switzerland) and fractionated according to the method of Huttner *et al.* (1983). For extraction experiments, the P3 pellet was homogenized by a Teflon homogenizer in a buffer solution containing 1 M NaCl or 1% Triton X-100 and centrifuged at 165 000 *g*. The samples were denatured and subjected to SDS–polyacrylamide gel electrophoresis. The proteins were then transferred onto an Immobilon Transfer Membrane (Millipore, Bedford, MA, USA) and processed for immunodetection.

Antibodies

The following primary antibodies were used: mouse monoclonal anti-drebrin (M2F6; Shirao and Obata 1986), mouse monoclonal anti-PSD-95 (7E3-1B8; Affinity BioReagents, Golden, CO, USA), mouse monoclonal anti-MAP2 (HM-2; Sigma, St. Louis, MO, USA), mouse monoclonal anti-Glial fibrillary acidic protein (anti-GFAP) (G-A-5; Sigma) and rabbit polyclonal anti-synapsin I (Chemicon). Polyclonal anti-spikar antibodies were raised against the C-terminal region of spikar (377–1208). The DNA fragment of spikar (377–1208) was subcloned into pET19b (Novagen, Madison, WI, USA). His^6-spikar (377–1208) was affinity-purified using a Ni^{2+} column (GE Health Care) according to the manufacturer's instructions. This His^6-spikar (377–1208) protein (2 mg) was used to immunize rabbits. The specificity of the anti-spikar antibodies was confirmed by western blotting (Figure S1).

Cell culture and transfection

Hippocampi were dissected from the fetuses of timed pregnant Wistar rats at embryonic day 18. The hippocampi were trypsinized and dissociated by trituration according to methods described previously (Takahashi *et al.* 2003). Briefly, cell suspensions were plated at a density of 5000 cells/cm^2 on coverslips coated with poly-L-lysine and incubated in minimum essential medium (Invitrogen) supplemented with 10% fetal bovine serum. Following cell attachment, the coverslips were transferred to a culture dish containing a glial monolayer sheet and maintained in serum-free minimum essential medium with B27 supplement (Invitrogen). Cytosine β-D-arabinofuranoside (10 μM; Sigma) was added to the cultures at 4 days *in vitro* (DIV) to inhibit glial proliferation.

Cells were transfected using the CaPO4 method (Details are provided in Figure S2). Microinjection was performed using a micromanipulator 5171 (Eppendorf, Hamburg, Germany).

HEK293 cells were cultured in Dulbecco's modified Eagle medium supplemented with 10% fetal bovine serum at 37°C in a 5% CO_2 atmosphere. Cells were transfected using Lipofectamine 2000 (Invitrogen).

RNA interference

To generate the RNA interference (RNAi) constructs used in this study, the following DNA oligonucleotides were annealed and subcloned into the pSUPERneo+GFP vector (OligoEngine, Seattle, WA, USA): 5′-gatccccggatcagttagagttaggattcaagagatcttagctctgactg atccttttggaaa-3′ and 5′-agcttttccaaaaaggatcagtcagagctaagatctcttgaatc ctaactctaactgatccggg-3′ (Spikar-shRNA-2); 5′-gatccccgttgatgcaagtag cagagttcaagagactttgctatttgcgtcaacttttggaaa-3′ and 5′-agcttttccaaaaagt tgacgcaaatagcaaagtctcttgaactctgctacttgcatcaacggg-3′ (Spikar-shRNA -3); 5′-gatccccgtgatgtgtggtttctgtattcaagagatgcagaaaccgtacatcac tttttg gaaa-3′ and 5′-agcttttccaaaaagtgatgtacggtttctgcatctcttgaata cagaaacc acacatcacggg-3′ (Drebrin-shRNA); 5′-gatccccccttacgttgagtacttcggttca agagatcgaagtactcagcgtaagttttta-3′ and 5′-agcttaaaaac ttacgctgagtact tcgatctcttgaaccgaagtactcaacgtaagggg3′ (Luciferase-shRNA). The targeted regions were not homologous to any other known genes, as confirmed by a BLAST search. The RNAi-resistant mutant of spikar-shRNA-3 was constructed by PCR using the following primers: 5′-ccacaagttgacgcagatcgcaaaggttgtcatc-3′ and 5′-gat-gacaaccctttgcgatctgcgtcaacttgtgg-3′. The RNAi-resistant mutant of drebrin was constructed by PCR using the following primers: 5′-gaaagtgatgtatggcttctgcagcgtc-3′ and 5′- gacgctgcagaagccatacatca ctttc-3′. A spikar-shRNA-3 construct was used to silence spikar. Cultured hippocampal neurons were transfected at 3 DIV with spikar-shRNA-3 to ensure that spikar expression would be suppressed during stage 5 of neuronal development (Dotti *et al.* 1988). Empty shRNA vector (pSUPERneo+GFP) was used as a control. The effect of the control vector on dendritic protrusions was similar to that of luciferase-shRNA vector (Figure S2). Another effective construct, spikar-shRNA-2, showed a reduction of the density of dendritic spines and filopodia similar to spikar-shRNA-3 (Figure S2). The efficiency of the drebrin knockdown construct has been described previously (Kato *et al.* 2012).

Electrophysiology

Whole-cell patch clamp recordings were performed with an Axopatch 200A amplifier (Axon Instruments, Union City, CA, USA) at 20–25°C. GFP-positive cultured hippocampal neurons from

17–19 DIV were identified using fluorescence microscopy (Olympus IX70, Tokyo, Japan) and used for electrophysiological studies. Patch pipettes were made from borosilicate glass capillaries (1.5 mm OD; Narishige, Tokyo, Japan) using a micropipette puller (P-87; Sutter Instrument, Novato, CA, USA). The resistance of the patch pipettes was 3–4 MΩ when filled with the pipette solution described below. The series resistance, 9.8 ± 0.6 MΩ, was not electronically compensated. The reference electrode was an Ag/AgCl electrode connected to the bath via an agar bridge filled with 150 mM NaCl. The potential of the pipette was corrected for the measured liquid junction potential (approximately 10 mV). Modified Tyrode solution was used as the external solution containing (in mM) 145 NaCl, 5 KCl, 2 $CaCl_2$, 1 $MgCl_2$, 10 glucose, and 10 HEPES (pH 7.4 with NaOH) plus 1 μM tetrodotoxin and 100 μM picrotoxin. The pipette solution contained (in mM) 122.5 Cs-gluconate, 17.5 CsCl, 8 NaCl, 0.2 EGTA, 2 ATP-Mg, 0.3 GTP, and 10 HEPES, and the pH was adjusted to 7.2 with Cs-OH. Whole-cell currents were recorded at 10 kHz after low-pass filtering at 2 kHz, and miniature excitatory postsynaptic currents (mEPSCs) were analyzed offline using Mini Analysis Software (Synaptosoft Inc., Decatur, GA, USA). We held the membrane potential of cultured neurons at −60 mV in voltage clamp and recorded the synaptic current.

Image analysis and statistics

Fluorescence images were acquired using a Zeiss Axioplan 2 microscope (Carl Zeiss, Jena, Germany) equipped with a CoolSnap fx CCD camera (Photometrics, Tucson, AZ, USA) and a 63 × oil-immersion, 1.4 NA (Carl Zeiss) objective at 25°C. The data were collected from two to three independent culture preparations, and analysis was performed by an experimenter blinded to the identity of the transfected constructs. Morphometric analysis and quantification were carried out using MetaMorph image analysis software (Molecular Devices, Sunnyvale, CA, USA). Neurons expressing GFP were imaged and quantified, and aspiny interneurons were excluded from the analysis. For each neuron, one or two dendrites 40–80 μm from the first branching point were selected and analyzed. For the morphological analysis of the dendritic protrusions, the maximum length and width of each protrusion of length 0.5–8 μm were measured manually (Figure S3a and b). Dendritic spines were defined as dendritic protrusions with a head or stubby type protrusion for which the length:width ratio was less than or equal to 2. Dendritic filopodia were defined as headless dendritic protrusions for which the length:width ratio was greater than 2. For the quantification of cluster number, clusters were defined as an immunostained region with a peak fluorescence level that was 2-fold greater than the averaged fluorescence level of the dendrites. For image analysis, statistical significance was determined with a Welch's *t*-test, Mann–Whitney U-test, Dunnett multiple comparison test, Tukey–Kramer multiple comparison test or Steel–Dwass multiple comparison test. Spine length and width were analyzed with the Kolmogorov–Smirnov test using SPSS software (SPSS, Chicago, IL, USA). p values less than 0.01 were considered statistically significant unless explicitly stated otherwise. For electrophysiology, statistical significance was determined with a Welch's *t*-test. Cumulative frequencies of mEPSC amplitude and inter-event interval were analyzed with the Kolmogorov–Smirnov test using Mini Analysis Software (Synaptosoft, Inc., NJ, USA). For reporter gene assays, all transfection studies were repeated at least twice in triplicate. Statistical analysis was performed using ANOVA followed by a post hoc comparison with Bonferroni's multiple range test. The data shown represent the mean values of triplicate transfections ± SEM.

Live-cell imaging

Live neurons were mounted in a modified 35-mm dish and imaged with a 40 × , 0.75 NA water-immersion objective (Carl Zeiss) in culture medium using the microscope described above. The images were captured within 5 min at 30°C.

Results

Spikar is a novel drebrin-binding transcriptional co-activator

To identify proteins that interact with drebrin, we performed a yeast two-hybrid screen using a rat brain cDNA library. We used the N-terminal region of drebrin (amino acids 1–233), which contains the actin-depolymerizing factor homology domain (ADF-H domain), as the screen bait. In the course of screening approximately 9×10^7 colonies, we isolated 89 independent clones. DNA sequencing of these clones showed that 64 of the 89 clones encoded the same protein. We termed this protein spikar (accession number AB074010); this name was derived from its unique subcellular localization (in spines and nuclei), as described in the following section. A computational analysis using the NCBI database indicated that spikar was a rat ortholog of human KIAA1125 (accession number AB032951) and human prkcbp1 (accession number AF233453) (Fossey *et al.* 2000), and that rat spikar could be further classified into three isoforms: spikar A (isolated in this study, accession number AB074010), spikar B (XP_215942), and spikar delta-C (isolated in this study, AB721962) (Fig. 1a). Spikar contains a NLS, Plant Homeo Domain, Bromo domain, nuclear receptor recognition sequence (a LXXLL motif), PWWP domain, coiled-coil domain, and a MYND domain (Fig. 1a). In the following experiments, we used spikar A unless explicitly stated otherwise.

BS69 is a spikar-like protein containing Plant Homeo Domain, Bromo, PWWP, coiled-coil, and MYND domains (Fig. 1a), and is a co-repressor of transcription (Masselink and Bernards 2000). Because spikar has a domain structure similar to BS69, we used a reporter gene assay to examine whether spikar affects transcription in the kidney fibroblast cell line CV1. When spikar was co-transfected with thyroid hormone receptor β1 (TRβ1), spikar potentiated TRβ1-mediated transcription of thyroid hormone response element in the presence of its ligand, triiodothyronine (T3; Fig. 1b). This activation was induced by T3 and was dependent on the spikar dose, indicating that spikar is a transcriptional co-activator for TRβ1 activity. This co-activator activity of

spikar was also detected in the neuroblastoma cell line N2A (Fig. 1c). In addition, spikar activated transcription mediated by the glucocorticoid receptor and estrogen receptor α (Figure S4a and b), both of which are expressed in the hippocampus (Tohgi *et al.* 1995). These data suggest that spikar acts as a transcriptional co-activator for nuclear receptors in these cells.

Spikar and drebrin interact at their N-terminal regions

We examined whether full-length drebrin binds to full-length spikar using a pull-down assay. His^6-drebrin specifically pulled down GFP-spikar from lysates of cells expressing GFP-spikar (Fig. 1d), demonstrating that drebrin can bind to spikar *in vitro*.

Next, we identified the spikar-binding region of drebrin using a yeast two-hybrid assay with drebrin (1–134) and drebrin (135–233). This assay showed that drebrin (1–134) bound to spikar, but drebrin (135–233) did not (Figure S5a). We then constructed a series of deletion derivatives of spikar to determine which region is required for the interaction with drebrin (1–134). Spikar (88–376), which contains the N-terminal region of spikar, bound strongly to drebrin (1–134). In contrast, spikar (384–1208) did not bind to drebrin. Because spikar (88–258) showed no significant binding activity, and spikar (146–376) showed only weak binding activity (Figure S5b), it appears that spikar (88–376) is necessary for strong drebrin-binding activity. A pull-down assay also demonstrated that full length HA-spikar as well as HA-spikar (1–376) bound to GST-drebrin (1–138), but HA-spikar (377–1208) did not (Fig. 1e). These data were consistent with the results of the yeast two-hybrid assay.

Immunochemical analysis of spikar expression

Immunoblot analysis of protein extracts prepared from various adult rat tissues showed that spikar was ubiquitously detected in the brain, spinal cord, thymus, liver, kidney, spleen, lung, heart, and testis, although the expression levels varied among the tissues (Fig. 1f). Notably, spikar expression levels were high in the thymus and spleen. In the central nervous system, spikar expression was greater in the cerebellum than the cerebral cortex and the spinal cord; spikar was hardly detected in glial cultures (Fig. 1g).

We next examined the subcellular distribution of spikar in cerebral cortex homogenate. Spikar was recovered mainly in the P1 fraction, which includes the cell nuclei. A small amount of spikar was also recovered in the P3 (microsomal) fraction (Fig. 1h). Drebrin was also recovered in the P3 fraction. To characterize the association of spikar with the P3 fraction, we treated the P3 fraction with detergent or a high salt solution. Spikar was detected in the cytosolic fraction formed by treatment with a high concentration of salt (1 M NaCl), whereas only faint amounts were detected in the cytosolic fraction formed by treatment with 1% Triton X-100 (Fig. 1i). As an internal control for membrane protein, we used an immunoglobulin binding protein (Bip), which was solubilized by 1% Triton X-100 but not by 1 M NaCl. These results indicate that spikar was recovered in the P3 fraction owing to protein–protein, but not protein–membrane, interactions.

Localization of spikar in neuronal nuclei and dendritic spines

Although spikar immunostaining was observed in most brain regions, intense immunostaining was particularly observed in regions with high cellular densities, such as the granule cell and pyramidal layers of the hippocampus and the granular layer of the cerebellum (Fig. 2a). Higher magnification images showed that spikar immunostaining was observed in cell nuclei as well as in a punctate staining pattern along dendrites (Fig. 2b and c).

Similarly, immunocytochemical analysis of hippocampal neurons cultured for 21 DIV showed that spikar immunostaining was present in cell nuclei and distributed along dendrites in a punctate pattern (Fig. 2d, left panels). Spikar immunopositive puncta were also stained with antibodies against drebrin (Fig. 2d, right panels). In the dendritic shaft of developing neurons, spikar was localized mainly in dendritic shaft at DIV 7 but in dendritic spines at DIV 14 (Figure S6). Furthermore, GFP-spikar expressed in cultured neurons accumulated in the nuclei and co-localized with drebrin (Fig. 2e). Because these data indicated that spikar is present in the spine and karyoplasm, we named the protein spikar.

Spikar knockdown decreases spine density during development

We next analyzed the role of spikar in dendritic spine formation. To reduce the expression of spikar, we used two short hairpin RNAs (shRNAs; pSUPER-RNAi-2 and -3) that targeted different regions of spikar mRNA. Both effectively suppressed the exogenous expression of myc-spikar in HEK293 cells (Fig. 3a). In cultured hippocampal neurons, the immunofluorescence intensity of endogenous spikar in the nucleus was decreased to 20% of control by 96 h after transfection with pSUPER-RNAi-3 (spikar-shRNA-3; Fig. 3b and c).

We knocked down spikar at 3 DIV and analyzed the effect on morphogenesis of dendritic protrusions at 16 DIV. We selected transfected neurons by GFP expression. Neuronal morphology was visualized by GFP fluorescence (Fig. 3d). Spikar knockdown (KD) caused a significant decrease in the density of dendritic spines and filopodia at 16 DIV (Control: 43.7 ± 1.8 spines/100 μm; 19.4 ± 1.2 filopodia/100 μm; Spikar KD: 20.6 ± 1.1 spines/100 μm; 11.6 ± 0.9 filopodia/100 μm; $^*p < 0.01$; Fig. 3e–g). Interestingly, cumulative frequency distributions showed no differences between the lengths and widths of dendritic spines in spikar-KD and control neurons (Fig. 3h, i), indicating that spikar KD does not affect spine morphology.

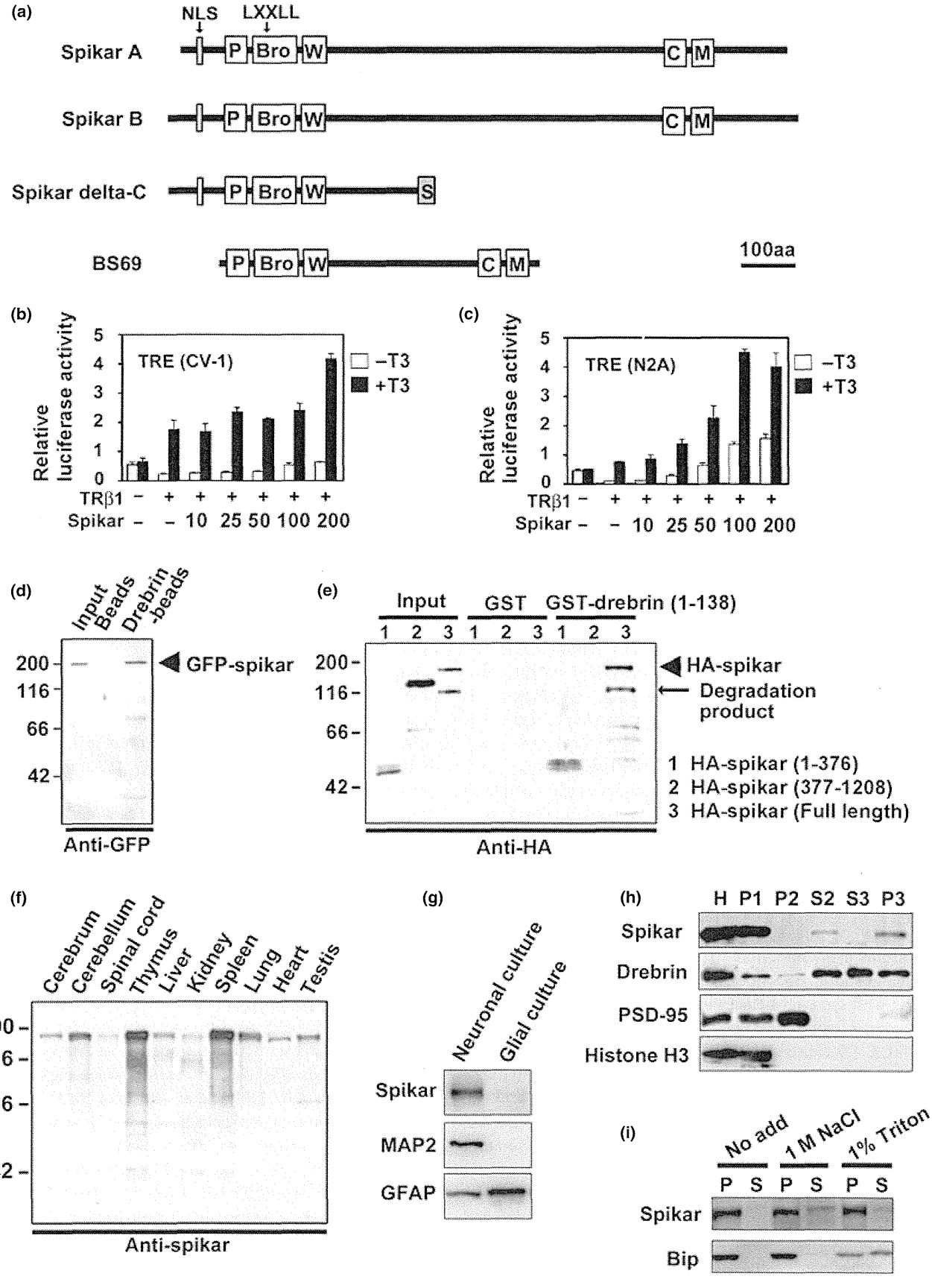
(a)
NLS
LXXLL
Spikar A
Spikar B
Spikar delta-C
BS69
P
Bro
W
C
M
S
100aa
(b)
Relative luciferase activity
TRE (CV-1)
−T3
+T3
TRβ1 − + + + + + +
Spikar − − 10 25 50 100 200
(c)
Relative luciferase activity
TRE (N2A)
−T3
+T3
TRβ1 − + + + + + +
Spikar − − 10 25 50 100 200
(d)
Input
Beads
Drebrin -beads
200
116
66
42
GFP-spikar
Anti-GFP
(e)
Input
GST
GST-drebrin (1-138)
1 2 3 1 2 3 1 2 3
200
116
66
42
HA-spikar
Degradation product
1 HA-spikar (1-376)
2 HA-spikar (377-1208)
3 HA-spikar (Full length)
Anti-HA
(f)
Cerebrum
Cerebellum
Spinal cord
Thymus
Liver
Kidney
Spleen
Lung
Heart
Testis
200
116
66
42
Anti-spikar
(g)
Neuronal culture
Glial culture
Spikar
MAP2
GFAP
(h)
H P1 P2 S2 S3 P3
Spikar
Drebrin
PSD-95
Histone H3
(i)
No add
1 M NaCl
1% Triton
P S P S P S
Spikar
Bip

Fig. 1 Characterization of spikar. (a) Schematic diagram of domain structures of spikar isoforms and BS69. P, Plant Homeo Domain (PHD) domain; Bro, Bromo domain; W, PWWP domain; C, Coiled-coil; M, MYND domain. (b, c) Spikar-activated nuclear-receptor-mediated transcription in CV-1 (b) and N2A cells (c). Cells were grown in the presence or absence of T3 (100 nM). (d) *In vitro* binding assay for the interaction between drebrin and spikar. Input: cell lysate containing GFP-spikar; Beads: samples precipitated with Ni-NTA beads; Drebrin-beads: samples precipitated with drebrin-conjugated beads. (e) GST pull-down assay for spikar and drebrin. Lysates of cells expressing each HA-spikar fragment (1, 1–376; 2, 377–1208; 3, 1–1208) were pulled down with GST-drebrin (1–134). (f) Western blotting of extracts from various tissues (200 μg wet weight for each). (g) Western blotting of lysates (5 μg protein) from neural and glial cultures. (h) Subcellular distribution of spikar. The protein extract (20 μg protein) from each fraction was analyzed by western blotting. H, homogenate; P1, cell nuclei and debris; P2, synaptosomal fraction; S2, non-synaptosomal fraction; S3, cytosolic fraction; P3, microsomal fraction. (i) The P3 fraction from rat cerebral cortices was treated with 1 M NaCl or 1% Triton X-100. The insoluble pellet (P) and supernatant (S) were analyzed by western blotting.

To assess the specificity of the effect of spikar KD on spine density, we performed a rescue experiment using RNAi-resistant spikar (myc-spikar^R), which is distributed to both the cytoplasm and nucleus (Figure S7a), or RNAi-resistant spikar with a mutated nuclear localization sequence (myc-mNLS-spikar^R), which does not enter the nucleus (Figure S7b). Expression of myc-spikar^R significantly increased the density of dendritic spines and filopodia (31.5 ± 1.0 spines/100 μm; 23.2 ± 0.8 filopodia/100 μm; $*p < 0.01$ vs. Spikar KD, Fig. 5e–g) of spikar-KD neurons. Expression of myc-mNLS-spikar^R also rescued the decrease in spine and filopodia densities (30.2 ± 1.1 spines/100 μm; 20.0 ± 0.8 filopodia/100 μm; $*p < 0.01$ vs. Spikar KD, Fig. 5e–g). In addition, we analyzed the dendritic arborization of spikar-KD neurons. Sholl analysis (Sholl 1953) showed that the arborization of the dendrites of spikar-KD neurons was significantly reduced (Figure S8). This phenotype was rescued by cotransfection of myc-mNLS-spikar^R (Figure S8).

Spikar knockdown decreases excitatory synapses

We examined whether spikar KD induces transformation of spine synapses into shaft synapses, or simply the disappearance of spine synapses. Immunocytochemical analysis showed that both PSD-95 and synapsin I clusters were significantly reduced in spikar-KD neurons (Control: PSD-95, 78.1 ± 4.3 clusters/100 μm; synapsin I, 125.4 ± 4.2 clusters/100 μm; Spikar KD: PSD-95, 50.0 ± 2.2 clusters/100 μm; synapsin I, 81.1 ± 2.9 clusters/100 μm; $*p < 0.01$, Fig. 4a and b). Synaptic PSD-95 clusters that were co-localized with synapsin I clusters were also reduced in spikar-KD neurons (Control, 63.0 ± 4.2 clusters/100 μm; Spikar KD, 34.0 ± 1.9 clusters/100 μm; $*p < 0.01$, Fig. 4b, right).

We next analyzed the spontaneous synaptic activity of spikar-KD neurons using electrophysiology (Fig. 4c). The amplitude of mEPSCs in spikar-KD neurons was 20.1 ± 2.0 pA, which was similar to that observed in control neurons (19.1 ± 2.3 pA; Fig. 4d). However, the inter-event interval of mEPSCs was significantly longer in spikar-KD neurons than in control neurons (568.8 ± 98.8 ms and 320.7 ± 63.5 ms, respectively, $p < 0.05$; Fig. 4e). These immunohistochemical and electrophysiological data indicate that spikar KD decreases the density of excitatory synapses, and suggest that spikar regulates the dendritic spine density with a concomitant change in the density of excitatory synapses.

Spikar knockdown facilitates the retraction of existing spines and suppresses the addition of new spines

To analyze whether spikar functions in spine stabilization or *de novo* spine formation, we followed the fate of spines using live-cell imaging (Fig. 5a). Cultured hippocampal neurons were transfected at 8 DIV with spikar-KD vector, and the same cells were analyzed at 16 and 22 DIV (a mature stage of cultured neurons) by imaging GFP fluorescence (Fig. 5b). During the 6-day period from 16 to 22 DIV, the number of retracted spines significantly increased (Control, 9.1 ± 1.0 spines/100 μm; Spikar KD, 15.5 ± 1.3; $*p < 0.01$), and the numbers of persistent and additional spines were significantly decreased (Control: persistent, 15.3 ± 0.9 spines/100 μm; addition, 20.5 ± 2.1; Spikar KD: persistent, 6.2 ± 1.6; addition, 4.2 ± 0.7; $*P < 0.01$) in spikar-KD neurons (Fig. 5c). These effects of spikar KD were blocked by the co-expression of myc-mNLS-spikar^R (retraction, 7.8 ± 0.7 spines/100 μm; persistent, 15.2 ± 1.2; addition, 18.9 ± 1.4; $*P < 0.01$ vs. Spikar KD, Fig. 5c). These results indicate that extranuclear spikar is required for the *de novo* formation and stabilization of dendritic spines.

Localization of spikar in dendritic spines depends on drebrin

To test whether the subcellular localization of spikar depends on drebrin, we performed a transfection study using HEK293 cells. When the cells were transfected with GFP-spikar, the GFP signal was localized to the nucleus and rarely observed in the cytoplasm (Fig. 6a). In contrast, when the cells were co-transfected with GFP-spikar and monomeric DsRED-drebrin, the percentage of cells in which GFP localized to the cytoplasm in addition to the nucleus was significantly increased (GFP-spikar, 3.2 ± 0.2%; GFP-spikar + monomeric DsRED-drebrin, 22.1 ± 1.5%; $*p < 0.01$, Fig. 6b and c). Therefore, the presence of drebrin facilitated the extranuclear distribution of spikar within the cells, suggesting that drebrin anchors spikar within the cytoplasm. When we

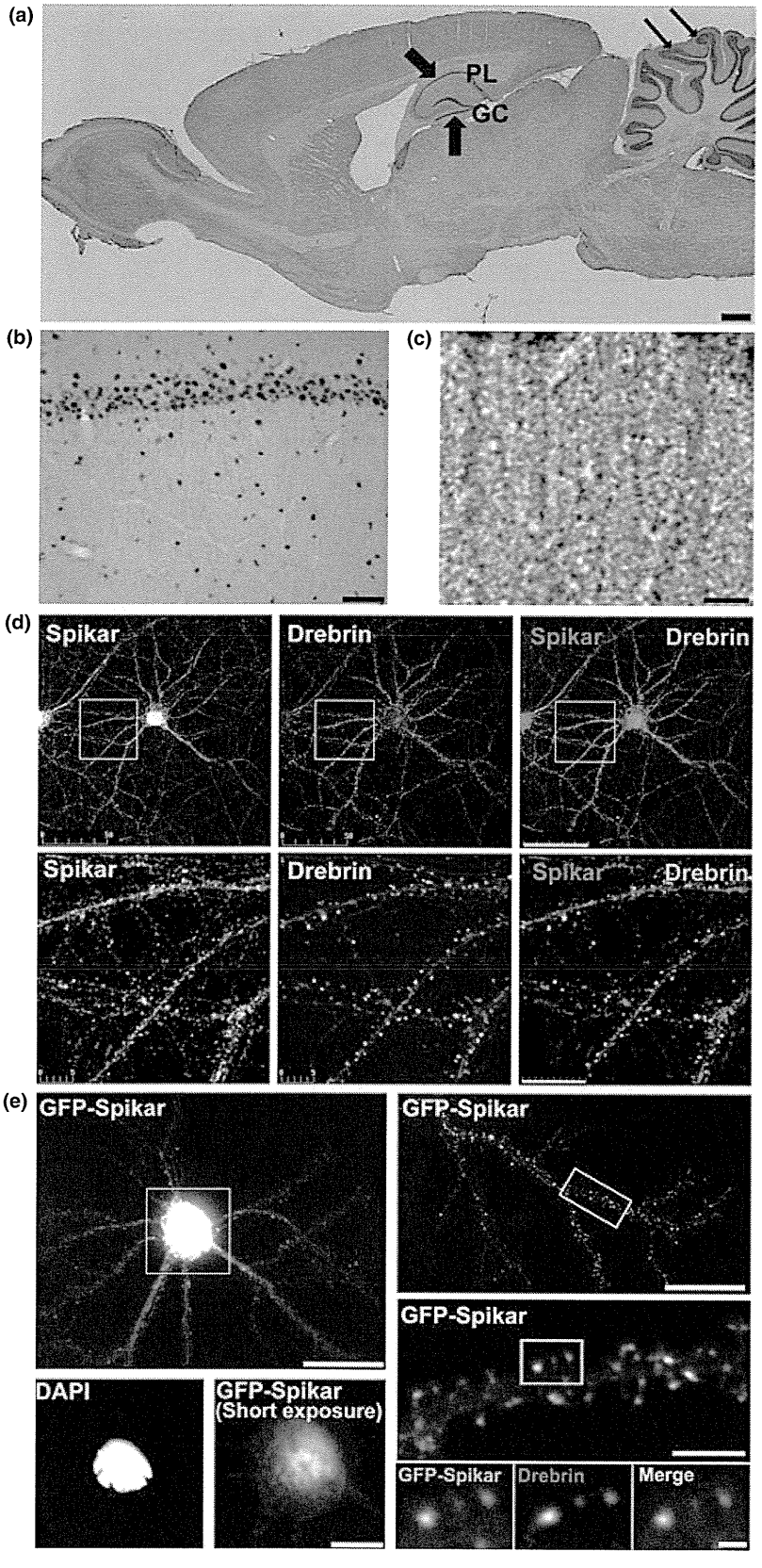

Fig. 2 Spikar is localized in neuronal nuclei and dendritic spines. (a–c) Immunohistochemical staining for spikar in adult rat brain. (a) Low magnification images of sagittal sections. Large arrows indicate granule cell and pyramidal layers of the hippocampus. Small arrows show the granular layer of the cerebellum. Scale bar, 1 mm. (b) Coronal section of hippocampal CA1 region. Scale bar, 50 μm (c) Higher magnification view of pyramidal neurons of the hippocampus. Note the punctate staining pattern observed in the dendritic region. Scale bar, 5 μm. (d) Cultured neurons were immunostained with spikar and drebrin antibodies at 21 DIV. The high magnification views (lower panels) show that spikar signals (red) overlap with drebrin signals (green) in dendritic spines. Scale bars, 50 μm (upper); 10 μm (lower). (e) Cultured neurons were microinjected with GFP-spikar at 21 DIV and analyzed at 22 DIV. Scale bars, 30 μm (upper); 5 μm (lower).

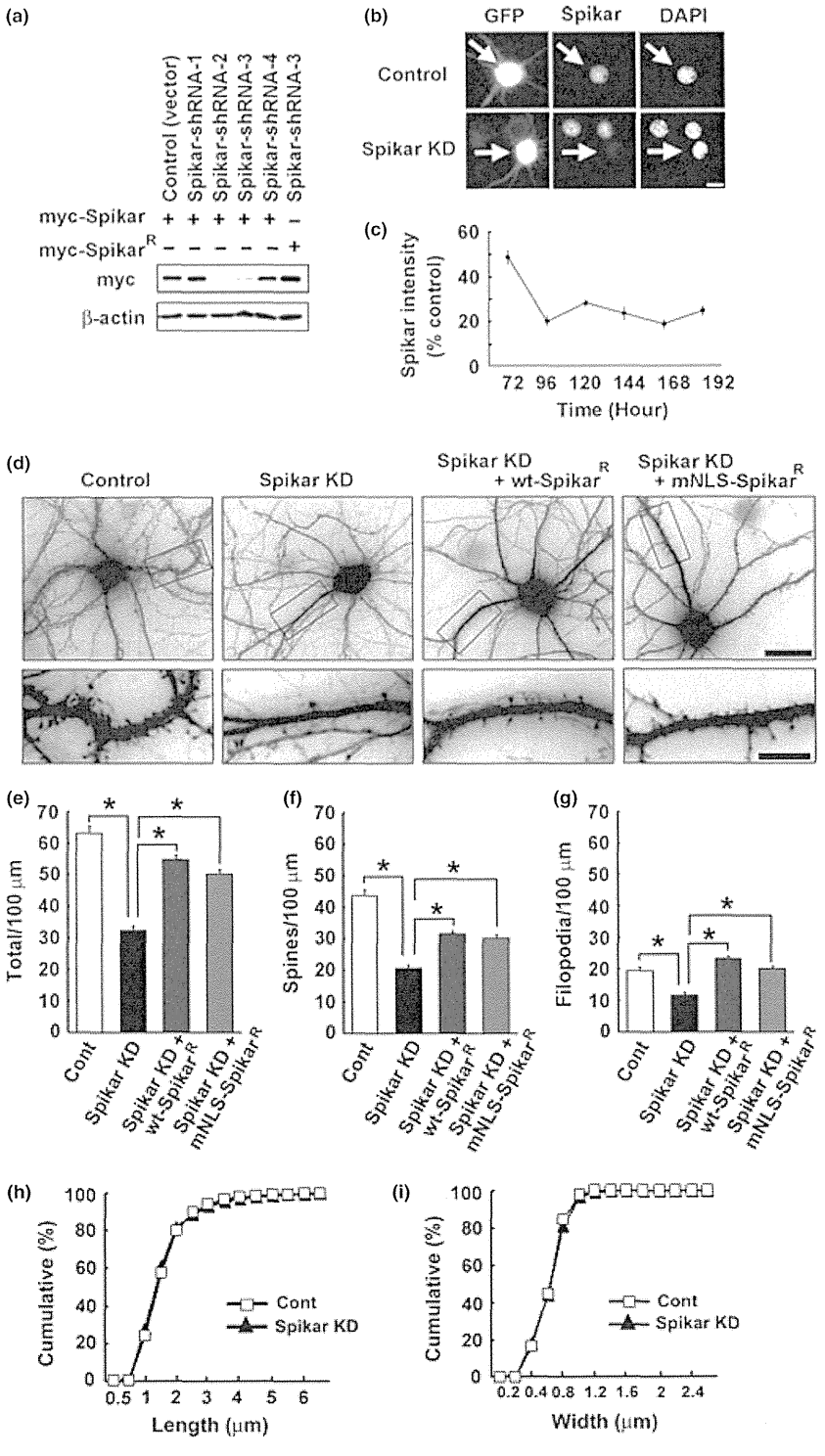

Fig. 3 Spikar knockdown reduces the density of dendritic spines and filopodia. (a) Efficacy of shRNAs. Note that myc-spikar^R is an RNAi-resistant mutant that is not affected by Spikar-shRNA-3. (b) Cultured hippocampal neurons were transfected with either an empty vector (control) or spikar-shRNA-3 and immunostained for spikar. Arrows indicate transfected neurons. Scale bar, 10 μm. (c) Timecourse of spikar knockdown (KD) in cultured hippocampal neurons. (d) Cultured neurons were transfected with an empty vector (cont), spikar-shRNA-3, spikar-shRNA-3+ myc-spikar^R, or spikar-shRNA-3+ myc-mutated nuclear localization sequence (mNLS)-spikar^R at 3 DIV and analyzed at 16 DIV. Scale bars, 30 μm (upper) and 10 μm (lower). (e–g) Quantification of effects of spikar KD on the density of total protrusions (spines and filopodia), spines, and filopodia. Data are presented as mean ± SEM ($n > 100$, $^*p < 0.01$, Tukey–Kramer test). (h, i) Cumulative frequency plots of the length and width of dendritic protrusions in neurons transfected with empty vector or spikar-shRNA-3. Data were collected from 1800–2500 protrusions from > 100 neurons for each group.

transfected myc-spikar into cultured hippocampal neurons, myc-spikar was localized to dendritic spines and the nucleus, similar to the expression pattern of endogenous spikar (Fig. 6d). In the dendritic spines, strong immunostaining of myc-spikar co-localized with strong drebrin signals. The immunofluorescence intensity of myc-spikar in the dendritic spines correlated with that of drebrin (correlation coefficient $r = 0.59$, $p < 0.01$, Fig. 6e).

Next, we examined whether drebrin KD changed the intracellular localization of myc-spikar in cultured neurons. We silenced the expression of drebrin using RNAi and then analyzed the localization of spikar. Myc-spikar was distrib-

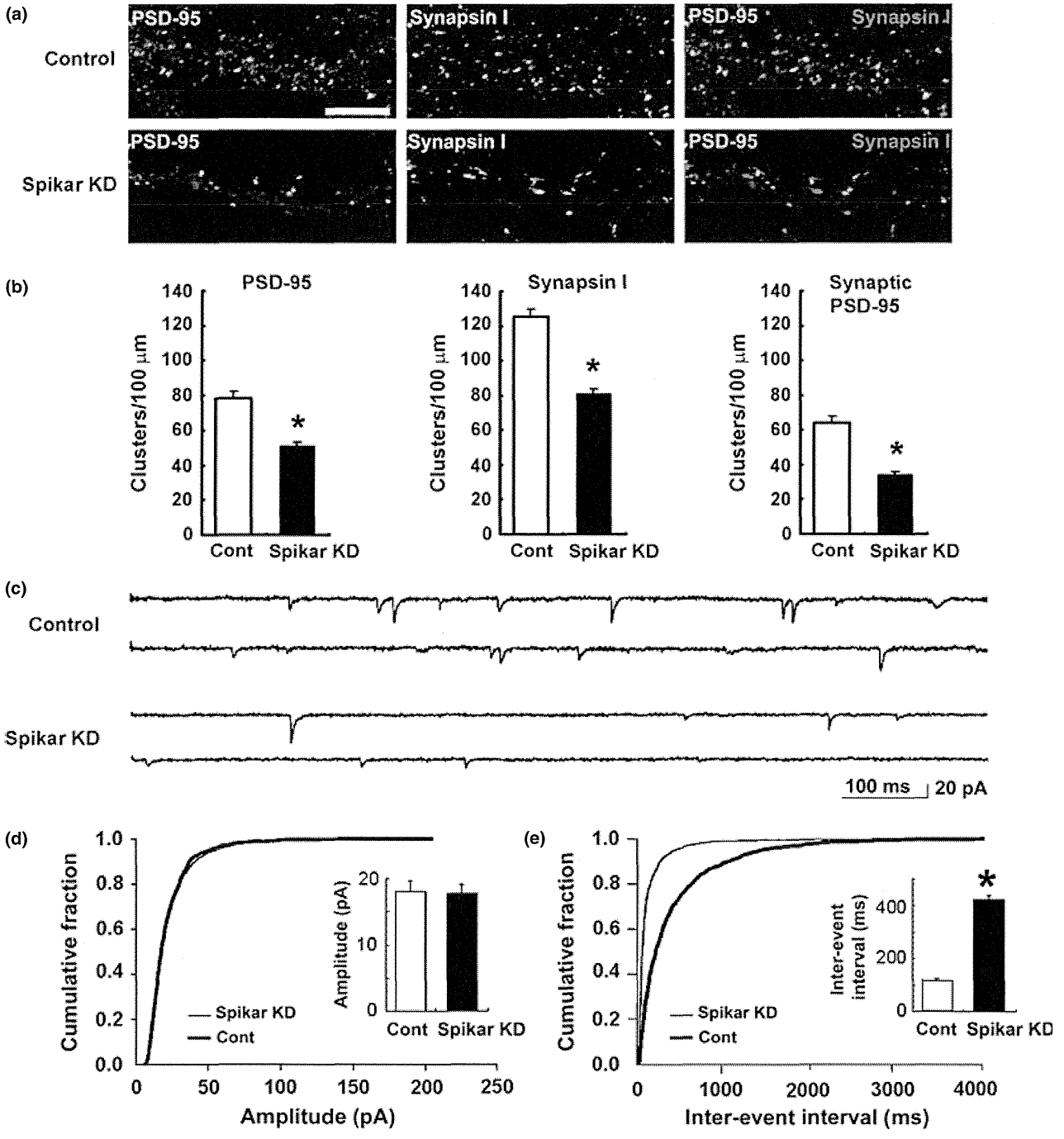

Fig. 4 Knockdown of spikar reduces excitatory synapses. (a) Cultured neurons were transfected with empty vector (cont) or spikar-shRNA-3 at 3 DIV and analyzed at 16 DIV. Spikar-knockdown (KD) neurons were immunolabeled for PSD-95 (green) and Synapsin I (red). Scale bar, 5 μm. (b) Quantification of cluster densities of PSD-95, Synapsin I, and PSD-95/Synapsin I. Data are presented as mean ± SEM (n = 58 and 64 for control and spikar KD, respectively, *p < 0.01, Welch's t-test). Excitatory synapses are defined as synapsin I-positive, PSD-95-positive clusters. (c) Representative recordings of miniature excitatory postsynaptic currents (mEPSCs) from control and spikar-KD neurons. (d, e) Quantification of mEPSC peak amplitudes and mEPSC inter-event intervals from control and spikar-KD neurons. Inset graphs show the mean ± SEM (n = 17 and 16 for control and spikar KD, respectively, *p < 0.01, Welch's t-test).

uted diffusely throughout the dendritic shafts in the drebrin-KD neurons but not in the control neurons (Fig. 6f). To assess the accumulation of spikar in the dendritic spines, the immunofluorescence intensities of myc-spikar were quantified in dendritic spines and shafts, and the ratios of spine to shaft intensities were calculated. The accumulation of myc-

spikar in spines was significantly inhibited by the loss of drebrin (Control spine/shaft intensity, 1.03 ± 0.03; Drebrin KD, 0.61 ± 0.01; $P < 0.01$) and was rescued by co-transfection with an RNAi-resistant drebrin mutant (drebrin^{R}) (1.86 ± 0.06, $*p < 0.01$ vs. Drebrin KD, Fig. 6g), indicating that the dendritic localization of spikar was dependent on drebrin. However, the C-terminal region of spikar (aa820-1041), which lacks drebrin-binding activity, accumulated in dendritic spines (Figure S9a). Furthermore, the spikar delta-C isoform, which has a drebrin-binding region but lacks the C-terminal region, was not localized in dendritic spines but was solely localized within the nucleus (Figure S9b). Therefore, binding of spikar to drebrin is not always correlated with dendritic spine localization.

Finally, we examined whether spikar affects drebrin localization at dendritic spines (Fig. 6h). In spikar-KD neurons, the percentages of drebrin-positive filopodia and spines in spikar-KD neurons were similar to those in control neurons (Fig. 6i). Furthermore, the drebrin immunofluorescence intensity within drebrin-positive spines was not affected by spikar KD (Fig. 6j). Together, these data indicate that drebrin localization does not depend on spikar, whereas spikar localization does depend on drebrin.

Overexpression of extranuclear spikar facilitates spine formation in a drebrin-dependent manner

To further investigate the function of spikar in the cytoplasm, we performed a spikar gain-of-function experiment by introducing mNLS-spikar into cultured neurons at 8 DIV and measuring the numbers of spines and filopodia at 13 DIV (Fig. 7a). Overexpression of mNLS-spikar significantly increased the densities of both spines and filopodia (Control: 14.9 ± 1.0 spines/100 μm; 33.8 ± 1.5 filopodia/100 μm; mNLS-spikar: 21.9 ± 1.3 spines/100 μm; 46.6 ± 2.0 filopodia/100 μm; $*p < 0.01$, Fig. 7b–d). We then examined whether the spine-formation activity of mNLS-spikar requires the presence of drebrin. We co-transfected mNLS-spikar and drebrin-shRNA into cultured neurons and measured the numbers of spines and filopodia. Drebrin KD (8–13 DIV) abolished the mNLS-spikar-induced increases in spine and filopodia density (Fig. 7b–d). The inhibition of mNLS-spikar function by drebrin KD was

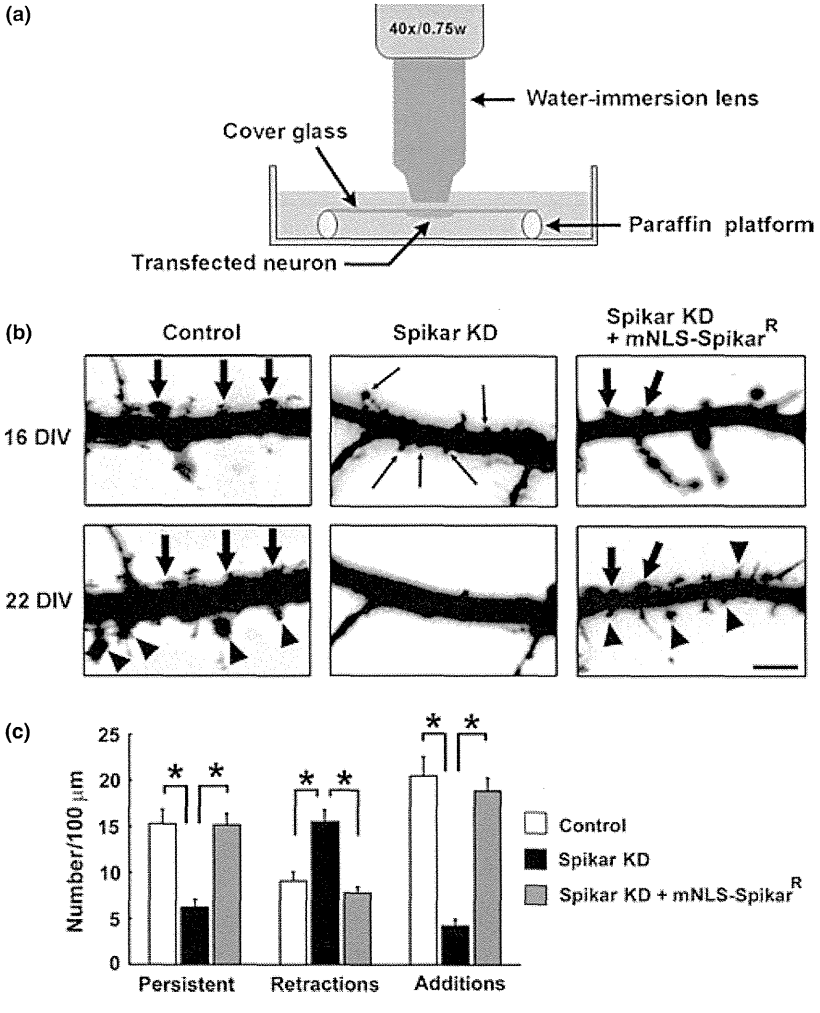

Fig. 5 Live-cell imaging of spikar-knockdown (KD) neurons. (a) Diagram of live-cell imaging method. (b) Cultured neurons were transfected at 8 DIV with empty vector (cont), spikar-shRNA-3, or spikar-shRNA-3+ myc-mutated nuclear localization sequence (mNLS)-spikar^{R}. Neurons expressing GFP were imaged at 16 and 22 DIV. Arrows indicate spines that were maintained, arrow heads indicate spines that were added, and thin arrows indicate spines that were retracted during the intervening 6-day period. Scale bars, 5 μm. (c) Quantification of the respective fates of spines. Data are presented as mean ± SEM (n = 30, 31, and 47 for control, spikar KD, and spikar KD + myc-mNLS-spikar^{R}, respectively, $*p < 0.01$, Tukey–Kramer test).

rescued by co-expression of drebrin^{R} (24.0 ± 1.6 spines/100 μm; 46.4 ± 2.8 filopodia/100 μm; *$p < 0.01$ vs. Drebrin KD + mNLS-spikar). Drebrin KD (8–13 DIV) did not affect the densities of spines and filopodia in the control culture (Fig. 7b–d), although prolonged drebrin-KD (3–16 DIV) decreased the density of spines and filopodia (Control: 45.4 ± 2.1 spines/100 μm; 23.5 ± 1.6 filopodia/100 μm; Drebrin KD: 31.6 ± 2.3 spines/100 μm; 17.7 ± 1.3 filopodia/100 μm; *$p < 0.01$, Figure S10a and b). These data indicate that extranuclear spikar facilitates spine formation, and that this effect requires drebrin.

Discussion

In this study, we identified a novel drebrin-binding protein that we named spikar. Spikar was localized in cell nuclei and acted as a transcriptional co-activator. Intriguingly, in neurons, spikar was localized at dendritic spines in addition to cell nuclei. Using a combination of RNAi knockdown and mNLS-spikar overexpression, we have shown that spikar is involved in the regulation of dendritic spine density.

Role of drebrin in subcellular localization of spikar

Because mNLS-spikar, which can bind to drebrin but lacks a normal NLS, is not localized in the nucleus, drebrin does not seem to be involved in the nuclear localization of spikar. However, drebrin overexpression increases the proportion of cytoplasmic spikar within HEK293 cells, and drebrin KD inhibits the dendritic accumulation of spikar. These data indicate that drebrin is involved in the localization of spikar in dendritic spines. The present study also demonstrates that protein–protein interaction plays a role in the recovery of spikar in the microsomal fraction, which contains drebrin. Moreover, the level of myc-spikar in dendritic spines is correlated with that of drebrin. These data suggest that drebrin anchors spikar in dendritic spines.

Our *in vitro* studies reveal that the N-terminal region of spikar binds to the ADF-H domain of drebrin. Although ADF-superfamily proteins generally bind to actin via the ADF-H domain (Lappalainen *et al.* 1998), drebrin binds to F-actin via the central actin-remodeling region (Hayashi *et al.* 1999; Grintsevich *et al.* 2010). Therefore spikar is not likely to compete with the interaction between drebrin and *F*-actin. We suggest that spikar is included in the drebrin-actin complex in dendritic spines via a direct protein–protein interaction between drebrin and spikar.

However, the delta-C isoform of spikar does not localize to dendritic spines despite the presence of a drebrin-binding domain. In addition, a C-terminal region (amino acids 820–1041) of spikar that does not bind to drebrin accumulates in dendritic spines. These data indicate that drebrin binding is not sufficient for spikar to be localized to dendritic spines, and that besides the direct protein–protein interaction between drebrin and spikar, another mechanism involving the C-terminal region of spikar must also play a role in the accumulation of spikar in dendritic spines.

Extranuclear spikar is involved in dendritic spine formation

The present study indicates that expression of either wild-type spikar or mNLS-spikar can rescue the decreased spine density of spikar-KD neurons. In addition, overexpression of mNLS-spikar increases the spine density of normal cells. Furthermore, our time-lapse imaging data indicate that mNLS-spikar increases the *de novo* formation of spines and decreases the retraction of existing spines in spikar-KD neurons. Because these data indicate that the expression level of extranuclear spikar relates directly to spine density, changes in transcription of other genes, which are likely to be induced by spikar, are not necessary for spine formation. However, we do not deny a possibility of involvement of spikar-mediated transcription in spine formation outright because mNLS-spikar did not rescue the spine density completely. Furthermore, the inhibitory effect of spikar-KD on dendritic branching might affect the formation of spines.

When spine density is decreased by spikar KD, the remaining spines show normal morphologies. In addition, although the frequency of AMPAR-mediated mEPSCs is decreased following spikar KD, the amplitude is not affected. Thus, it is suggested that spikar is involved in the formation

Fig. 6 Drebrin mediates spikar anchoring at dendritic spines. (a) HEK293 cells were transfected with GFP-spikar or GFP-spikar + mDsRED-drebrin. Cytoplasmic GFP-spikar was selectively imaged by subtracting the DAPI signal from GFP images (Subtraction). Scale bar, 50 μm. (b) High magnification image of a co-transfected cell. Scale bar, 20 μm. (c) The ratio of cells possessing cytoplasmic spikar to the total number of transfected cells was significantly increased in the presence of drebrin ($n = 30$ fields, *$p < 0.01$, Mann–Whitney U-test). (d) Cultured neurons were transfected with myc-spikar, and immunostained with myc-spikar (red) and drebrin (green). Scale bars, 30 μm (upper) and 5 μm (lower). (e) Immunofluorescence intensities of myc-spikar and drebrin in spines were significantly correlated ($r = 0.59$, $p < 0.01$). (f) Cultured hippocampal neurons were transfected at 8 DIV with empty vector (cont), or drebrin-shRNA + myc-spikar, or drebrin-shRNA + myc-spikar + HA-drebrin^{R}. Scale bar, 5 μm. (g) Quantification of the effect of drebrin knockdown (KD) on spine localization of myc-spikar. Data are presented as mean ± SEM ($n > 400$ spines from 30 neurons, *$p < 0.01$, Steel–Dwass test). (h) Cultured neurons were transfected with empty vector (control) or spikar-shRNA-3 (3–16 DIV). Transfected neurons were immunolabeled with antibody for drebrin. Scale bar, 5 μm. (i, j) Quantification of effects of spikar KD on the percentage of drebrin-positive protrusions (i) and the immunofluorescence intensity of drebrin (j). Data are presented as mean ± SEM ($n = 50$ for each group).

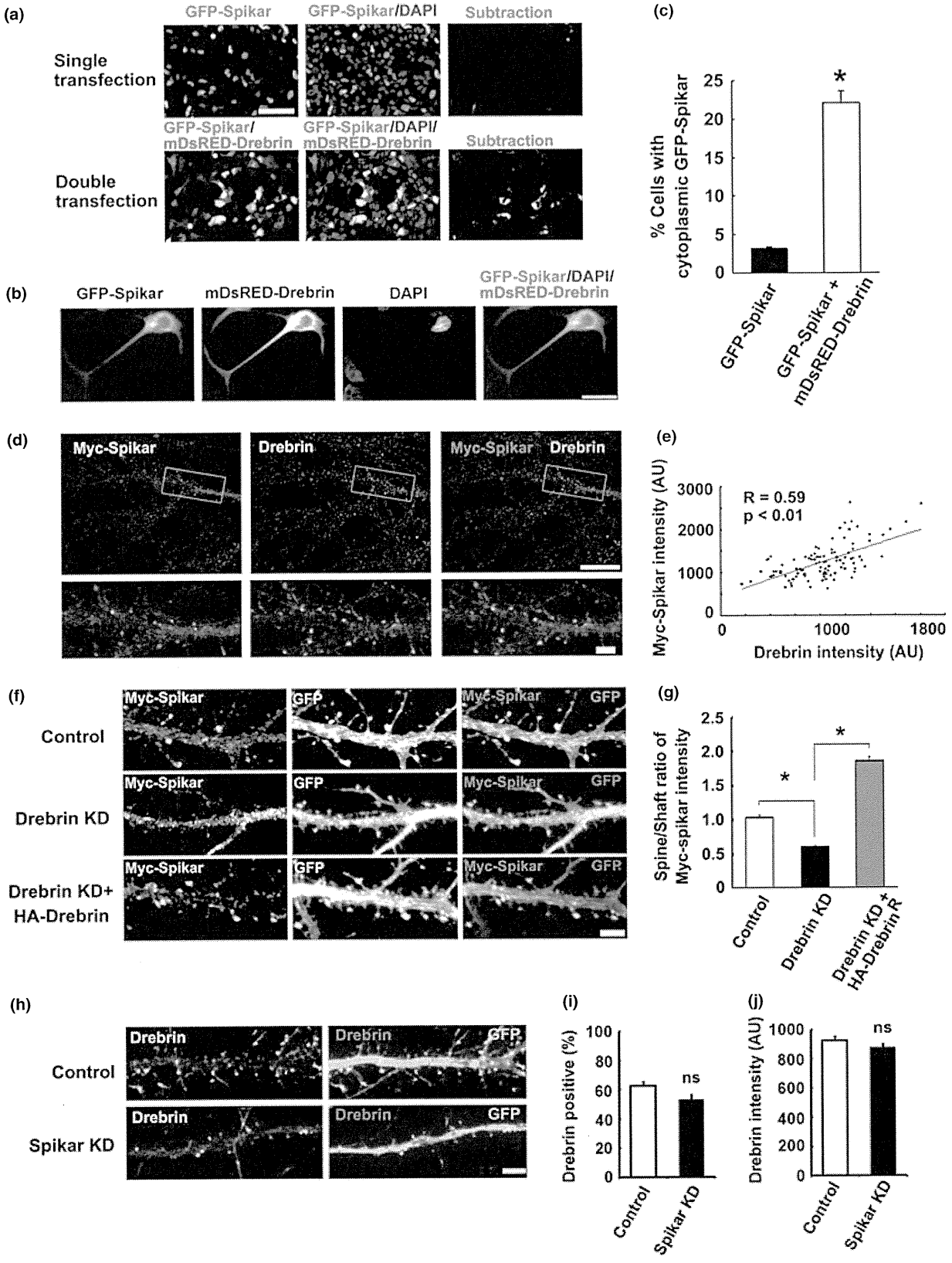
(a)
GFP-Spikar
GFP-Spikar/DAPI
Subtraction
Single transfection
GFP-Spikar/ mDsRED-Drebrin
GFP-Spikar/DAPI/ mDsRED-Drebrin
Subtraction
Double transfection
(b)
GFP-Spikar
mDsRED-Drebrin
DAPI
GFP-Spikar/DAPI/ mDsRED-Drebrin
(c)
% Cells with cytoplasmic GFP-Spikar
25
20
15
10
5
0
*
GFP-Spikar
GFP-Spikar + mDsRED-Drebrin
(d)
Myc-Spikar
Drebrin
Myc-Spikar Drebrin
(e)
Myc-Spikar intensity (AU)
3000
2000
1000
0
R = 0.59
p < 0.01
0
1000
1800
Drebrin intensity (AU)
(f)
Control
Drebrin KD
Drebrin KD+ HA-Drebrin
Myc-Spikar
GFP
(g)
Spine/Shaft ratio of Myc-spikar intensity
2.5
2.0
1.5
1.0
0.5
0
*
*
Control
Drebrin KD
Drebrin KD + HA-Drebrin R
(h)
Control
Spikar KD
Drebrin
GFP
(i)
Drebrin positive (%)
100
80
60
40
20
0
ns
Control
Spikar KD
(j)
Drebrin intensity (AU)
1000
800
600
400
200
0
ns
Control
Spikar KD

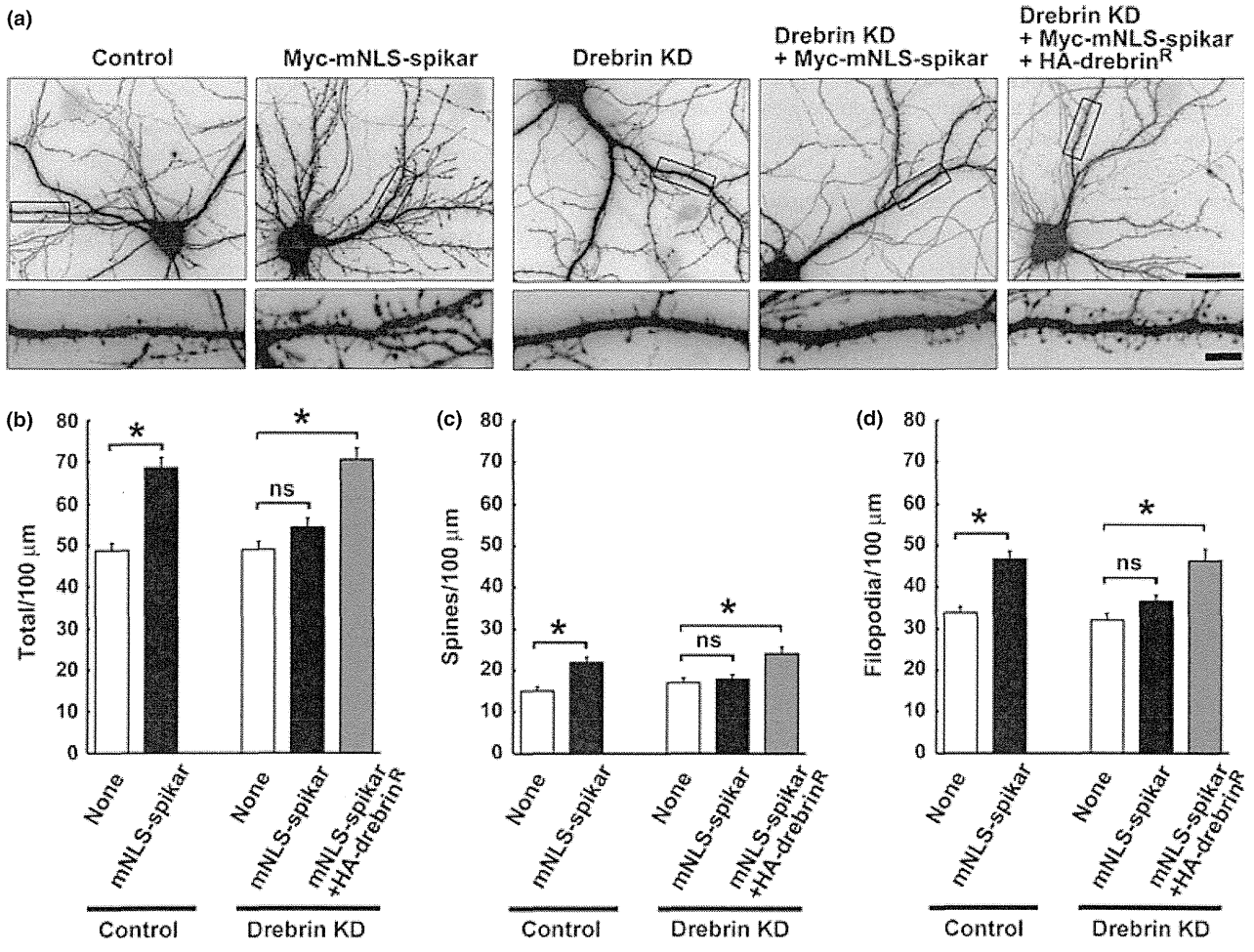

Fig. 7 Effect of extranuclear spikar overexpression is inhibited by drebrin knockdown (KD). (a) Cultured neurons were transfected after 8 DIV with empty vector (control), empty vector + myc-mutated nuclear localization sequence (mNLS)-Spikar, drebrin-shRNA, drebrin-shRNA + myc-mNLS-Spikar, or drebrin-shRNA + myc-mNLS-Spikar + HA-drebrin^R. GFP images were analyzed at 13 DIV. Scale bars, 30 μm (upper); 5 μm (lower). (b–d) Quantification of spine and filopodia density for each experimental condition. Data are presented as mean ± SEM ($n = 55$ for each group, $^*p < 0.01$, Tukey–Kramer test).

and stabilization of dendritic spines, but it is not involved in the function of mature spines.

Role of drebrin–spikar interaction in spine formation

Interestingly, overexpression of mNLS-spikar did not increase spine density in drebrin-KD neurons. This suggests that drebrin-mediated anchoring of spikar through protein-protein interaction at dendritic spines is necessary for increasing spine density. An alternative explanation is that the decrease in spine density caused by drebrin KD counteracts the increase induced by spikar overexpression. We and others have previously shown that drebrin KD inhibits spine formation (Takahashi *et al.* 2006; Biou *et al.* 2008). In fact, we detected a significant decrease in spine density in longer duration (3–16 DIV) drebrin KD. Therefore, spikar might function in a different regulatory pathway from drebrin. However, we did not detect any decrease in spine density in a drebrin-KD experiment of the same duration (8–13 DIV) as the mNLS-spikar overexpression experiment. This result indicates that the likelihood of the latter possibility is low, although it is not known why shorter term drebrin KD (8–13 DIV) did not lead to a decrease in spine density similar to prolonged drebrin KD (3–16 DIV). The reduction of drebrin expression in drebrin KD (8–13 DIV) neurons might be sufficient to block *de novo* spine formation induced by overexpressed mNLS-spikar, but not enough to decrease the spine density compared with the reduction in drebrin KD (3–16 DIV).

While the present study indicates that spikar KD does not affect spine morphology, our previous study demonstrated that drebrin KD does alter spine morphology (Takahashi *et al.* 2006). It has been reported that drebrin accumulates at nascent excitatory postsynaptic sites (Aoki *et al.* 2005) before the accumulation of PSD-95 (Takahashi *et al.* 2003)

and drebrin is suggested to play a pivotal role in forming a unique stable actin structure at postsynaptic sites (Shirao and Gonzalez-Billault 2013). Spikar may be recruited to the actin structure by binding to drebrin, and consequently functions in the spikar-mediated spine density regulatory pathway. In this context, other proteins recruited to the stable actin structure could mediate the morphological changes in dendritic spines, in a manner distinct from the spikar-mediated regulatory pathway.

Several molecules have been reported to be involved in dendritic spine formation and stabilization (McMahon and Diaz 2011). Diacylglycerol kinase (DGK)ζ is a DGK isoform that is enriched at excitatory synapses. DGKζ KD is known to reduce spine stability and density without changing spine morphology (Kim *et al.* 2009). Furthermore, the loss of DGKζ decreases the frequency of mEPSCs without affecting their amplitudes (Kim *et al.* 2009). Because these morphological and electrophysiological phenotypes of DGKζ KD are similar to those of spikar KD, it is suggested that spikar and DGKζ might be involved in a similar pathway regulating dendritic spine formation and stabilization, although an interaction between DGKζ and drebrin has not been reported.

Some cell adhesion molecules are also involved in dendritic spine formation and stabilization. Knockdown of N-cadherin reduces the stability of dendritic spines (Mendez *et al.* 2010), and a dominant-negative disruption of leukocyte common antigen-related (LAR) receptor protein tyrosine phosphatase function increases the retraction of existing spines and decreases *de novo* spine formation (Dunah *et al.* 2005). Although these phenotypes are similar to those of spikar KD, unlike spikar KD, the functional inhibition of N-cadherin or LAR results in formation of smaller dendritic spines. Therefore, spikar is likely to be involved in a different regulatory pathway from N-cadherin or LAR.

Acknowledgments

We thank Dr Ryoki Ishikawa for His6-drebrin. T7 work was supported by Grants-in-Aid for Young Scientists (15700285, 18700306, 21700340) and a Grant-in-Aid for Scientific Research (19200029) from the Japan Society for the Promotion of Science (JSPS). All authors declare that they have no conflict of interest.

Supporting information

Additional supporting information may be found in the online version of this article at the publisher's web-site:

Appendix S1. The expression vectors for TRβ1 and ERα (Takeshita *et al.* 1998), and GR (Iwasaki *et al.* 2001) have been described previously.

Figure S1. (a) The spikar antibody recognized GFP-spikar as a single band at approximately 200 kDa, demonstrating that the spikar antibody specifically recognized spikar protein.

Figure S2. (a) Cultured neurons were transfected with an empty vector (control), luciferase-shRNA, or spikar-shRNA-2 at 3 DIV, and analyzed at 16 DIV.

Figure S3. (a) Higher magnification image of dendritic spines. The neuron is transfected with GFP. Scale bar, 2 μm. (b) Illustration of panel (a).

Figure S4. (a, b) Spikar activated transcription mediated by the glucocorticoid receptor (GR) and estrogen receptor α (ERα) in CV-1 cells.

Figure S5. (e, f) Interaction between drebrin and spikar were assayed by HIS3 induction in the yeast two-hybrid system.

Figure S6. (a, b) Immunofluorescence localization of spikar in cultured GFP-transfected neurons at two developmental stages (7 DIV and 14 DIV).

Figure S7. (a, b) Cultured hippocampal neurons were transfected at 8 DIV with myc-spikar (a) or myc-mNLS-spikar (b), and immunostained with anti-myc antibody at 16 DIV.

Figure S8. Cultured neurons were transfected with an empty vector (cont), spikar-shRNA-3, spikar-shRNA-3 + myc-spikarR, or spikar-shRNA-3 + myc-mNLS-spikarR at 3 DIV and analyzed at 16 DIV.

Figure S9. (a) Cultured neurons were transfected with GFP-spikar (820-1041) at 8 DIV and analyzed at 16 DIV. GFP-spikar (820-1041), which does not bind to drebrin, was localized in dendritic spines. Scale bar, 5 μm.

Figure S10. (a) Cultured neurons were transfected with empty vector (control) or drebrin-shRNA at 3 DIV and analyzed at 16 DIV. Prolonged drebrin KD decreased the density of dendritic spines and filopodia. Scale bars, 30 μm (upper); 5 μm (lower).

References

Aoki C., Sekino Y., Hanamura K., Fujisawa S., Mahadomrongkul V., Ren Y. and Shirao T. (2005) Drebrin A is a postsynaptic protein that localizes in vivo to the submembranous surface of dendritic sites forming excitatory synapses. *J. Comp. Neurol.* **483**, 383–402.

Biou V., Brinkhaus H., Malenka R. C. and Matus A. (2008) Interactions between drebrin and Ras regulate dendritic spine plasticity. *Eur. J. Neurosci.* **27**, 2847–2859.

Dotti C. G., Sullivan C. A. and Banker G. A. (1988) The establishment of polarity by hippocampal neurons in culture. *J. Neurosci.* **8**, 1454–1468.

Dunah A. W., Hueske E., Wyszynski M., Hoogenraad C. C., Jaworski J., Pak D. T., Simonetta A., Liu G. and Sheng M. (2005) LAR receptor protein tyrosine phosphatases in the development and maintenance of excitatory synapses. *Nat. Neurosci.* **8**, 458–467.

Ethell I. M. and Pasquale E. B. (2005) Molecular mechanisms of dendritic spine development and remodeling. *Prog. Neurobiol.* **75**, 161–205.

Fossey S. C., Kuroda S., Price J. A., Pendleton J. K., Freedman B. I. and Bowden D. W. (2000) Identification and characterization of PRKCBP1, a candidate RACK-like protein. *Mamm. Genome* **11**, 919–925.

Gorlich A., Zimmermann A. M., Schober D., Bottcher R. T., Sassoe-Pognetto M., Friauf E., Witke W. and Rust M. B. (2012) Preserved morphology and physiology of excitatory synapses in profilin1-deficient mice. *PLoS ONE* **7**, e30068.

Grintsevich E. E., Galkin V. E., Orlova A., Ytterberg A. J., Mikati M. M., Kudryashov D. S., Loo J. A., Egelman E. H. and Reisler E. (2010) Mapping of drebrin binding site on F-actin. *J. Mol. Biol.* **398**, 542–554.

Hayashi K. and Shirao T. (1999) Change in the shape of dendritic spines caused by overexpression of drebrin in cultured cortical neurons. *J. Neurosci.* **19**, 3918–3925.